

MASTER OF SCIENCE THESIS

Nonlinear Geometric Control of a Quadrotor with a Suspended Load

N.N. Vo

July 6, 2017

Nonlinear Geometric Control of a Quadrotor with a Suspended Load

MASTER OF SCIENCE THESIS

For obtaining the degree of Master of Science in Mechanical
Engineering at Delft University of Technology

N.N. Vo

July 6, 2017

The work in Master of Science Thesis was supported by Alten. Their cooperation is hereby gratefully acknowledged.



Delft University of Technology

Copyright © Delft Center for Systems and Control
All rights reserved.

DELFT UNIVERSITY OF TECHNOLOGY
DELFT CENTER FOR SYSTEMS AND CONTROL

The undersigned hereby certify that they have read and recommend to the Faculty of Mechanical, Maritime and Materials Engineering for acceptance a thesis entitled “**Nonlinear Geometric Control of a Quadroptor with a Suspended Load**” by **N.N. Vo** in partial fulfillment of the requirements for the degree of **Master of Science**.

Dated: July 6, 2017

Supervisor:

dr.ir. T. Keviczky

Readers:

Dr. J Alonso-Mora

A. Sharifi Kolarijani

ir. B. van Vliet

Abstract

A Quadrotor is a type of Unmanned Aerial Vehicle that has received an increasing amount of attention recently with many applications including search and rescue, surveillance, supply of food and medicines as disaster relief and object manipulation in construction and transportation. An interesting subproblem of transportation, is the control of the position of a cable suspended load. The challenge is in the fact that the Quadrotor-Load system is highly nonlinear and under-actuated. The load cannot be controlled directly and has a natural swing at the end of each Quadrotor movement.

This thesis presents a Nonlinear Geometric Control approach for the position tracking of a cable suspended load. In this work the dynamical model of the Quadrotor-Load system is limited to the subsystem where the cable tension is non-zero, which is analogous to modeling a rigid link between the Quadrotor and Load. Furthermore, an introduction is given on Geometric Mechanics, which applies differential geometric techniques to systems modeling and control, based on the geometric properties of the system. The Quadrotor-Load system dynamics are modeled on so called manifolds, smooth nonlinear geometric configuration spaces. Analyzing these geometric structures with the principles of differential geometry allows modeling in an unambiguous coordinate-free dynamic fashion, while avoiding the problem of singularities that would occur on local charts. Tracking error functions are defined on these same spaces, making it possible to design almost globally defined controllers.

The main goal of this thesis is to investigate the possibilities and limitations of Nonlinear Geometric Control by evaluating the performance of tracking different load trajectories. A backstepping approach is applied to generate a cascaded structure with multiple nonlinear Geometric controllers, allowing control of several flight modes that are responsible for the control of 1) Quadrotor attitude, 2) Load attitude and 3) Load position. A Linear Quadratic Regulator is derived to compare control performance. Simulations are presented and the results of both the linear and nonlinear controller are discussed.

Bart: Objective little bit more explicit, suggestion: The main goal of this thesis is to investigate the possibilities and limitations of Nonlinear Geometric Control by evaluating the performance of tracking different trajectories. To compare control performance, a linear Quadratic Regulator is derived.

At least it should be an eyecatcher for the reader to know what the objective of the thesis is

Nam: Nog meer aanpassen?

Acknowledgements

I would like to thank my supervisors dr.ir. T. Keviczky from Delft Center of Systems and Control, and ir. B. van Vliet from Alten Nederland B.V. for their assistance during my research and the writing of this thesis. I would also like to thank all colleagues from Alten and TU Delft for their time and advice.

Delft, University of Technology
July 6, 2017

N.N. Vo

Table of Contents

Abstract	v
Acknowledgements	vii
1 Introduction	1
1-1 Aim and Motivation	2
1-2 Organization of the Report	3
2 Dynamic Model	5
2-1 Geometric Mechanics	5
2-2 Modeling Assumptions	8
2-3 Quadrotor-Load Model	10
3 Control Design	15
3-1 Nonlinear Geometric Control	15
3-2 Quadrotor Attitude Tracking	19
3-3 Load Attitude Tracking	20
3-4 Load Position Tracking	21
3-5 Stability Analysis	21
4 Experiment	23
4-1 Procedure	23
4-2 Trajectories	24
4-2-1 Case A	24
4-2-2 Case B	24
4-2-3 Case C	25
4-3 Setup	25

5	Results	29
5-1	Case A	30
5-2	Case B	33
5-3	Case C	35
5-4	Conclusion	38
6	Conclusions and Future Work	39
6-1	Summary and Conclusions	39
6-2	Recommendations for Future Work	39
6-2-1	Investigate Implementation	39
6-2-2	Minimum Snap Trajectory Generation	40
6-2-3	Hybrid System	41
A	Appendix	43
A-1	Derivation of Equations of motion	43
A-1-1	Load Dynamics	43
A-2	LQR controller	43
A-2-1	Modeling	43
A-3	Classical Modeling	44
A-4	Derivation Error dynamics	46
A-5	Figures	47
	Bibliography	49
	Acronyms	53

List of Figures

2-1	Configuration Space of a 2-link arm	6
2-2	A manifold locally resembles a Euclidean space	7
2-3	Manifolds and Tangent Spaces	7
2-4	Quadrotor model representation	9
2-5	Quadrotor with Load model representation	11
3-1	Nonlinear Geometric Control Loop of the QR-Load system [15]	17
3-2	Transport map $\mathcal{T}(R, R_d)$	18
4-1	Desired Load Position Case A	24
4-2	Desired Load Position Case C	25
4-3	LQR control design	26
5-1	Controller Comparison Case A	30
5-2	Results Nonlinear Geometric Control Case A	32
5-3	Controller Comparison Case B	33
5-4	Results Nonlinear Geometric Control Case B	34
5-5	Controller Comparison Case C	35
5-6	Results Nonlinear Geometric Control Case C	37
A-1	Model representation	45
A-2	Simulink Command Filter	47

List of Tables

2-1	Modeling assumptions	10
4-1	Modeling Parameters	25
4-2	Controller Gains	27

Chapter 1

Introduction

A Quadrotor (**QR**) is a type of Unmanned Aerial Vehicle (**UAV**) that has received an increasing amount of attention recently with many applications being actively investigated. Possible applications include search and rescue, surveillance, reliable supply of food and medicines as disaster relief and object manipulation in construction and transportation. It has already proven itself useful for many tasks like multi-agent missions, mapping, explorations, transportation and entertainment such as acrobatic performances.

The inspiration for this research is build upon the idea of creating a system of multiple autonomous **QRs** for a cooperative towing task. The advantage of such systems for object manipulation is the increased reach and the possibility to reduce complexity of the individual robot, decrease cost over traditional robotic systems and high reliability. One can think of examples in nature, where individuals coordinate, cooperate and collaborate to perform tasks that they individually can not accomplish. Redundancy makes development of fail safe control methods possible and can extend the capabilities of a single robot.

Considering a multi-agent task, one can think of multiple **QRs** assisting in the transportation of a common load. This cooperation can be executed in many ways, but this research focuses on **QRs** with a cable-suspended load in motion. The suspended object naturally continues to swing at the end of every movement. In case a residual motion can result in damage or in order to avoid obstacles and path following, an accurate positioning is required. Reducing the oscillation, or controlling the position of the suspended load might be necessary, but is challenging in the fact that this cable-suspended system is under-actuated. Possible objectives are minimizing the oscillations of the load during or after motion, minimizing the time to position the load, trajectory tracking, trajectory generation and obstacle avoidance.

1-1 Aim and Motivation

The aim is to control the position of a suspended load using a QR. Before considering multiple QRs, it is important to investigate the possibilities of a single QR with load system. Hence, in this research a single QR is considered for the transportation of a cable suspended load, which will exert additional forces and torques on the QR. This is a challenging control problem in the fact that the QR system is under-actuated. Adding a suspended load will add extra DOFs and oscillations of the load occur at the end of every movement.

The system can be divided into two subsystems. The first subsystem is where the cable tension is non-zero and the distance between the QR and the load is defined by the cable length. Both QR and load are coupled as one system. The second subsystem is where the cable tension is zero, such that the QR and load in free fall are two separate decoupled systems. This research focuses on the first subsystem, such that the cable tension is non-zero. In order to control both subsystems, hybrid control must be applied, which is considered out of the scope of this research.

Former work on attitude control of QR and/or load often relies on linear control methods such as PID, MPC and LQR control. The dynamics are linearized around an equilibrium point, describing the system dynamics by a set of linear differential equations. The control of a QR-Load system is a very specific case and scarcely investigated. Former work includes MPC [1] and LQR control approaches, where an optimal control strategy is used to minimize the swing of the load.

The reason that linear control near an equilibrium state is commonly applied, is partly to avoid difficulties that come with modeling and controlling the non-linearities of the system. However, linear control limits the system to small angle movements, as the optimization will not allow large angles that deviate to far from the linearized point. For applications that require fast aggressive maneuvers, this type of modeling and control will not be sufficient. Nonlinear control systems are often governed by nonlinear differential equations and are able to represent the dynamics in a more realistic manner. Nonlinear control approaches to minimize the load swing includes a Model Based Algorithm controller applied by [2].

Bart: These problems. Which problems in the previous sentence are you referring to?

Nam: optimization problems

Nonlinear Geometric Control is a nonlinear model based control technique based on a modeling approach involving the concepts of differential geometry. This results in a globally defined coordinate-free dynamical model, while preventing issues regarding singularities, and enabling the design of controllers that offer almost-global convergence properties.

Former work includes a nonlinear geometric control of a QR [3, 4] and nonlinear geometric control of the load position, load attitude and QR attitude of a QR-Load system [5, 6, 7]. Nonlinear Geometric Control for QR systems is rarely found in literature, despite the advantageous properties of differential geometry.

This motivates to investigate the potential and limitations of a rarely used nonlinear Geometric Control approach, and to investigate the performance of a load transportation maneuver,

when compared to a commonly used linear control strategy.

Different aspects involving the modeling and control for the QR-Load system must be investigated, for it can be expected that the non-linearity will have a great influence in the representation of the dynamics and the stability, accuracy and type of the control design. It is possible to investigate which advantages or disadvantages this nonlinear approach has compared to a linear approach, in terms of stability and performance.

1-2 Organization of the Report

In this first chapter, a brief introduction of the subject is given and the problem is described. This is followed by discussing the aim, motivation and contributions of this thesis for this research. The organization of the report is as follows.

In Chapter 2 the dynamics of the QR-Load system is described by the laws of kinematics and the application of Newton's laws or Lagrangian mechanics. Geometric Mechanics is used to understand and derive the system's equations of motion in order to allow nonlinear geometric controller design and analysis. The system configuration space is described on a differentiable manifold using the tools of Differential geometry, instead of using the tools of Euclidean geometry, where the system dynamics evolve in a three dimensional space. In contrast with classical modeling techniques, geometric modeling results in a compact, unambiguous and coordinate-free model.

bart: Also possible? declare a bit more. It's not some coincidence you're describing differential geometry. Actually, it's one of the key stones of geometric control, thus your thesis.

Nam: Anders geformuleerd

Describing the system dynamics on nonlinear manifolds allows the design of nonlinear geometric controllers on these same manifolds. The control design is presented in Chapter 3. The controller has a cascaded structure, allowing the control of several flight modes that are accountable for the control of different degrees of freedom.

Chapter 5 describes the experiments that are done to investigate the abilities and performance of a nonlinear Geometric Control design. Different tracking objectives are defined in order to compare the performance between an LQR control design and a nonlinear Geometric Control design. The results are presented and findings are discussed.

Bart:Suggestion: change test to compare? Because the compare part is not yet mentioned

Nam: beter?

In the final chapter a summary of the thesis is given, followed by the conclusions that were made based on the results of the research. Finally, recommendations are given which could serve as an starting point for future work.

Chapter 2

Dynamic Model

A mathematical model of the system needs to be derived in order to simulate and study the effects of nonlinear Geometric Control. In Section 2-1, an introduction is given about Geometric Mechanics. This is a modern description of the classical mechanics from the perspective of Differential Geometry, which is a discipline in mathematics that studies manifolds and their geometric properties, using the tools of calculus.

The assumptions that are applied to simplify the model are shortly discussed in Section 2-2. Next, in Section 2-3 a dynamical model of the QR-Load system is obtained with Geometric Mechanics, resulting in a compact, coordinate-free, unambiguous representation of the dynamics, described on nonlinear manifolds.

2-1 Geometric Mechanics

For the derivation of the equations of motions, traditional modeling methods often parameterize the rotations in a local coordinate system. This can be done with Euler Angles, and despite this parametrization might result in singularities, this is a commonly used method to describe rotations. There are 24 possible sets of Euler angles and many different conventions are used, which introduces ambiguity. The definition of Euler angles is not unique and a sequence of rotations is not commutative. Therefore, Euler angles are never expressed in terms of the external frame, or in terms of the co-moving rotated body frame, but in a mixture.

Euler angles are kinematically singular since the transformation from their time rates of change to the angular velocity vector is not globally defined. Furthermore, when angular errors are large, the difference in Euler angles is no longer a good metric to define the orientation error. Hence, the error is rather written as the required rotation to get from the current to a desired orientation, which can be achieved by considering geometric properties of the system.

In Geometric Mechanics the configuration space of systems is a *group manifold* instead of a Euclidean space. The kinetic and potential energies are expressed in terms of this configuration space and their tangent spaces. It explores the geometric structure of a Lagrangian-

or Hamiltonian system through the concepts of vector calculus, linear algebra, differential geometry, and nonlinear control theory. Geometric mechanics provides fundamental insights into the nonlinear system mechanics and yields useful tools for dynamics and control theory.

An example is given of a simple 2-link arm, to illustrate different representations of a configuration space, see Figure 2-1. Let the configuration of the arm be defined in a Cartesian coordinate system. The position of end-effector E is defined as a coordinate in the x, y -plane, which can be calculated with arm lengths l_1, l_2 and the angles θ_1, θ_2 . This can be seen in Figure 2-1a. The gray configuration illustrates a singularity, because the definition of one point has multiple solutions.

Next, let the configuration be defined by the rotations q_1 and q_2 , as shown in Figure 2-1b. The configuration space is represented as a geometric shape called a *torus*, a smooth manifold where every configuration is mapped uniquely, as shown in Figure 2-1c. This allows the configuration to be represented globally.

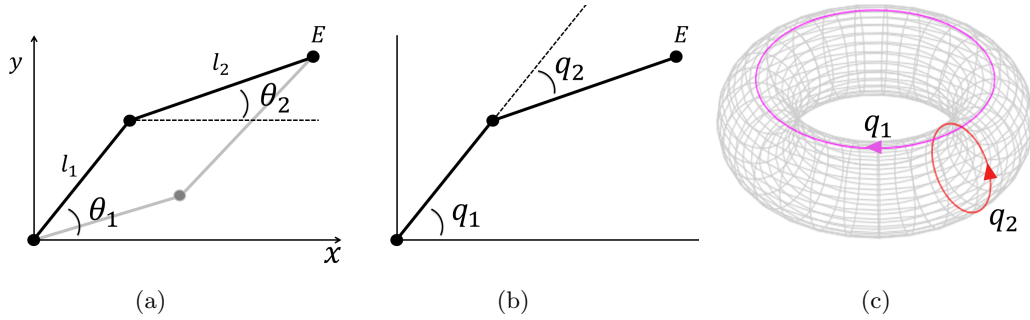


Figure 2-1: Configuration Space of a 2-link arm

Manifolds The fundamental object of differential geometry is a manifold. A manifold is a mathematical space, a collection of points, that locally resembles Euclidean space near each point. Examples are a plane, a ball, a torus and a sphere. Manifolds are important objects in mathematics and physics because they allow more complicated structures to be expressed and understood in terms of the relatively well-understood properties of simpler spaces. Each point of an n -dimensional manifold has a neighborhood that is homeomorphic to the n -dimensional Euclidean space, meaning that there is a continuous function describing the relation between these spaces, illustrated in Figure 2-2.

A *differentiable manifold* is a smooth and continuous manifold and is locally similar enough to a linear space to allow to do calculus. One can define directions, tangent spaces, and differentiable functions on such a manifold.

Taking the derivative at a point on a manifold is equivalent to a *tangent vector* at that point. Meaning that derivatives are conceptually equivalent to an infinitesimally short tangent vector. Each point of an n -dimensional differentiable manifold has a tangent space, which is an n -dimensional Euclidean space consisting of all the tangent vectors of all curves that pass through that point.

As an example, the manifold S^2 is represented as a sphere, with a tangent space at point x ,

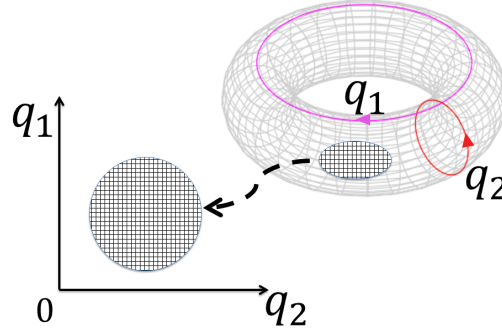
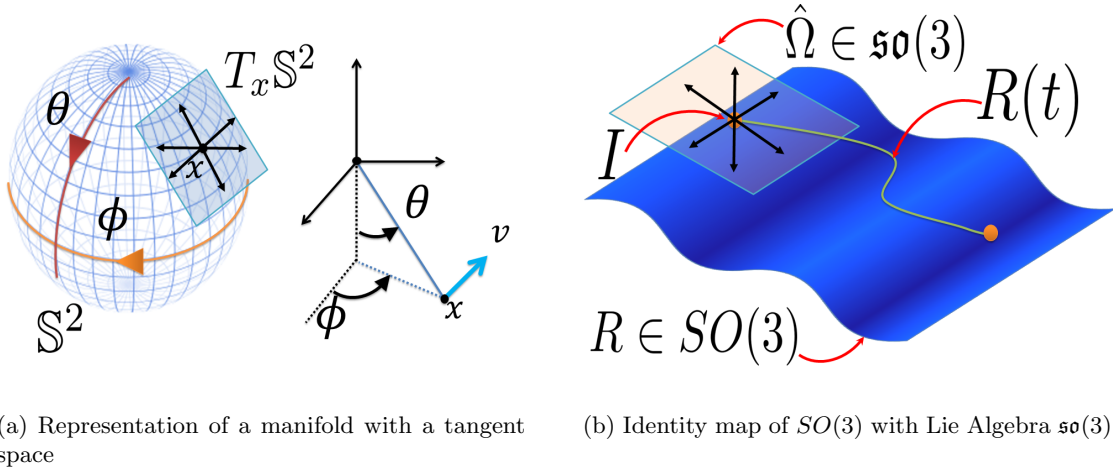


Figure 2-2: A manifold locally resembles a Euclidean space

denoted by $T_x\mathbb{S}^2$, see Figure 2-3a. This illustrates the concept of the relation between v , the derivative of x in Cartesian space, and the tangent space in on the manifold.



(a) Representation of a manifold with a tangent space

(b) Identity map of $SO(3)$ with Lie Algebra $\mathfrak{so}(3)$

Figure 2-3: Manifolds and Tangent Spaces

Geometric Configuration Spaces Several methods exist to describe rotations, such as *Euler Angles*, quaternions or rotation matrices. The main disadvantages of Euler angles are that some functions have singularities and they are a less accurate measure for the integration of incremental changes in attitude over time, compared to other methods. To avoid these problems, in Geometric Mechanics the rotations are expressed in rotation matrices to provide a global representation of the attitude of a rigid body, by mapping a representation of vectors expressed in $\{\mathcal{B}\}$ to a representation expressed in $\{\mathcal{I}\}$ [8, 9].

The configuration of the **QR** attitude is expressed in a rotation matrix R in the Special Orthogonal Group $SO(3)$ defined as

$$SO(3) \triangleq \{R \in \mathbb{R}^{3 \times 3} | RR^T = I_{3 \times 3}, \det(R) = 1\} \quad (2-1)$$

where $SO(3)$ is the group of all rotations about the origin of a 3-D Euclidean space, which preserves the origin, Euclidean distance and orientation.

Every rotation has a unique inverse rotation and the identity map satisfies the definition of a rotation. The elements of *Lie Algebra* $\mathfrak{so}(3)$, a property associated with $SO(3)$, are the elements of the *tangent space* of $SO(3)$ at the identity element, see Figure 2-3b. These elements define the relation between the rotation R and its derivative \dot{R} , such that

$$\dot{R} = R\hat{\Omega} \quad (2-2)$$

For $n \in \mathbb{N}$, $\mathfrak{so}(n)$ is the vector space of skew-symmetric matrices in $\mathbb{R}^{n \times n}$ and defined as

$$\mathfrak{so}(n) \triangleq \{S \in \mathbb{R}^{n \times n} | S^T = -S\} \quad (2-3)$$

The hat map $\wedge : \mathbb{R}^3 \rightarrow \mathfrak{so}(3)$ is an isomorphism between \mathbb{R}^3 and the set of 3×3 skew symmetric matrices, such that $\hat{x}y = x \times y$ for any $x, y \in \mathbb{R}^3$. The vee map $\vee : \mathfrak{so}(3) \rightarrow \mathbb{R}^3$, and is the inverse isomorphism of the hat map. Several properties of the hat map are

$$\hat{x}y = x \times y = -y \times x = -\hat{y}x, \quad (2-4)$$

$$\text{tr}[A\hat{x}] = \frac{1}{2}\text{tr}[\hat{x}(A - A^T)] = -x^T(A - A^T)^\vee, \quad (2-5)$$

$$\hat{x}A + A^T\hat{x} = (\{\text{tr}[A]I_{3 \times 3} - A\}x)^\wedge, \quad (2-6)$$

$$R\hat{x}R^T = (Rx)^\wedge, \quad (2-7)$$

for any $x, y \in \mathbb{R}^3$, $A \in \mathbb{R}^{3 \times 3}$, and $R \in SO(3)$. The mapping between the body angular velocity vector $\Omega \in \mathbb{R}^3$ and $\hat{\Omega} \in \mathfrak{so}(3)$ is written as

$$\hat{\Omega} = \begin{bmatrix} 0 & -\Omega_3 & \Omega_2 \\ \Omega_3 & 0 & -\Omega_1 \\ -\Omega_2 & \Omega_1 & 0 \end{bmatrix}, \quad \begin{bmatrix} 0 & -\Omega_3 & \Omega_2 \\ \Omega_3 & 0 & -\Omega_1 \\ -\Omega_2 & \Omega_1 & 0 \end{bmatrix}^\vee = \Omega \quad (2-8)$$

The load attitude is expressed as a unit vector q , which points from $\{\mathcal{B}\}$ to the load. The configuration space is a *two-sphere* \mathbb{S}^2 defined as

$$\mathbb{S}^2 \triangleq \{q \in \mathbb{R}^3 | q \cdot q = 1\} \quad (2-9)$$

The plane tangent to the sphere at q is the tangent space

$$T_q\mathbb{S}^2 \simeq \{\omega \in \mathbb{R}^3 | q \cdot \omega = 0\} \quad (2-10)$$

where ω is the angular velocity of the suspended load.

2-2 Modeling Assumptions

The QR model representation is shown in Figure 2-4. Three Cartesian coordinate frames are defined:

- The body-fixed reference frame $\{\mathcal{B}\}$ (Body Frame)
with unit vectors $\{\mathbf{b}_1, \mathbf{b}_2, \mathbf{b}_3\}$ along the axes

- The ground-fixed reference frame $\{\mathcal{I}\}$ (Inertial Frame)
with unit vectors $\{\mathbf{e}_1, \mathbf{e}_2, \mathbf{e}_3\}$ along the axes
- The intermediary frame $\{\mathcal{C}\}$, ($\{\mathcal{I}\}$ rotated by the yaw angle ψ)
with unit vectors $\{\mathbf{c}_1, \mathbf{c}_2, \mathbf{c}_3\}$ along the axes

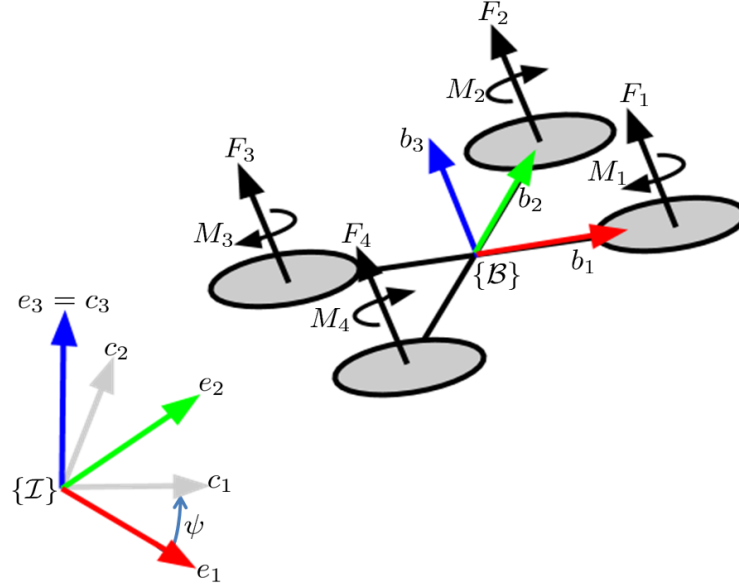


Figure 2-4: Quadrotor model representation

The complex dynamics of the rotors and their interactions with drag and thrust forces are represented by a simplified model. The angular speed ω_i of rotor i , for $i = 1, 2, 3, 4$, generates a force F_i parallel to the direction of the rotor axis of rotor i , given by

$$F_i = \left(\frac{K_v K_\tau \sqrt{2\rho A}}{K_t} \omega_i \right)^2 \simeq b\omega_i^2 \quad (2-11)$$

where K_v, K_t are constants related to the motor properties, ρ is the density of the surrounding air, A is the area swept out by the rotor, K_τ is a constant determined by the blade configuration and parameters, and b is the thrust factor.

The torque around the axis of rotor i , generated due to drag is given by

$$M_i = \frac{1}{2} R \rho C_D A (\omega_i R)^2 \simeq d\omega_i^2 \quad (2-12)$$

where R is the radius of the propeller, C_D is a dimensionless constant, and d is the drag constant.

The required rotor speeds ω_i can be calculated for a given desired total thrust f and total moment $M = [M_\phi \ M_\theta \ M_\psi]^T$, by solving the following equation

$$\begin{bmatrix} f \\ M_\phi \\ M_\theta \\ M_\psi \end{bmatrix} = \begin{bmatrix} b & b & b & b \\ 0 & -lb & 0 & lb \\ lb & 0 & -lb & 0 \\ -d & d & -d & d \end{bmatrix} \begin{bmatrix} \omega_1^2 \\ \omega_2^2 \\ \omega_3^2 \\ \omega_4^2 \end{bmatrix} \quad (2-13)$$

where l is the distance from the rotor to the QR's CM and M_ϕ, M_θ, M_ψ denote the moments around the x, y, z -axis in $\{\mathcal{B}\}$, respectively.

Table 2-1 shows the assumptions that are used for modeling the QR-Load system, simplifying the complexity of the model.

<p>Modeling assumptions Quadrotor model</p> <ul style="list-style-type: none"> • The structure of the QR is rigid and symmetric. Elastic deformations and shock (sudden accelerations) of the QR are ignored. • The mass distribution of the QR is symmetrical in the x-y plane. • The inertia matrix is time-invariant. • Aerodynamic effects acting on the QR are neglected. Blade flapping, Turbulence, Ground Effects. • The air density ρ around the QR is constant. • The propellers are rigid \Rightarrow The thrust produced by rotor i is parallel to the axis of rotor i. • Drag factor d and thrust factor b are approximated by a constant. Thrust force F_i and moment M_i of each propeller is proportional to the square of the propeller speed.
<p>Modeling assumptions Quadrotor-Load model</p> <ul style="list-style-type: none"> • The cable is modeled as a rigid and massless cable. • The cable is connected to a friction-less joint at the origin of the body-fixed. • The tension in the cable is considered to be non-zero. This implies that the QR-Load subsystem, consisting of a separate QR and Load in free fall, is disregarded. • Aerodynamic effects acting on the load are neglected. reference frame.

Table 2-1: Modeling assumptions

2-3 Quadrotor-Load Model

The Quadrotor-Load model consists of two subsystems, the first where the cable tension is zero, and the second where the cable tension is non-zero. In this research, the focus is only on the subsystem where the cable tension is non-zero. The QR-Load model is shown in Figure 2-5, where the unit vector $q \in \mathbb{S}^2$ gives the direction from the QR to the Load expressed in $\{\mathcal{B}\}$. The position of the QR and Load are related by

$$x_Q = x_L - Lq \quad (2-14)$$

where $x_Q \in \mathbb{R}^3$ is the position of the QR's CM, $x_L \in \mathbb{R}^3$ is the position of the load, and L is the length of the cable.

Considering the properties of the system, the QR is described as a rigid body with six degrees of freedom, driven by forces and moments. Rigid body dynamics and optimal control problems

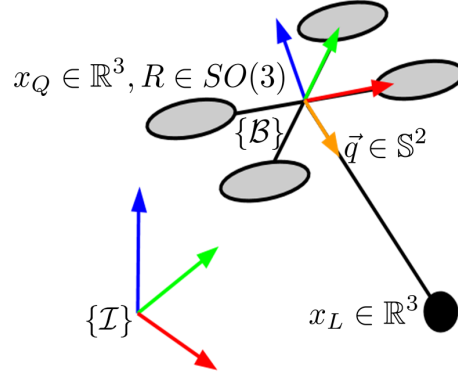


Figure 2-5: Quadrotor with Load model representation

are studied, and their geometric features are incorporated in [10]. The focus lies on obtaining geometric properties of the dynamics of rigid bodies, how their configuration can be described and how these geometric properties are utilized in control system analysis and design.

The configuration of the **QR** can be described by the location of the **QRs CM**, $x_Q \in \mathbb{R}^3$, described in the Euclidean space w.r.t. $\{I\}$ and by the orientation of $\{B\}$, also called attitude, w.r.t. $\{I\}$ evolving on a nonlinear space $R \in SO(3)$.

The configuration of the load can be described by its location $x_L \in \mathbb{R}^3$ w.r.t. $\{I\}$, evolving in Euclidean space, and attitude $q \in \mathbb{S}^2$ evolving on a nonlinear space called *two-sphere*.

To conclude, all the dynamics of the **QR**-Load system can be globally expressed on the Special Orthogonal Group $SO(3)$, *two-sphere* \mathbb{S}^2 and Special Euclidean Group $SE(3)$. This results in a compact notation of the equations of motion, making the large amount of trigonometric functions unnecessary, that Euler angles normally introduce.

Euler-Lagrange To develop the Euler-Lagrange equations for mechanical systems that evolve on manifolds, an approach developed by [10, 11, 12, 13] is applied. The basic idea is to express the variations of the curves evolving on \mathbb{S}^2 and $SO(3)$ in terms of the Lie Algebra $\mathfrak{so}(3)$, see Equations 2-28. This approach is based on Hamilton's principle, which states that the evolution of a physical system is a solution of the functional equation given by

$$\frac{\delta S}{\delta \mathbf{x}(t)} = 0 \quad (2-15)$$

where \mathbf{x} defines the configuration space. S is the action integral, defined as

$$S = \int_{t_1}^{t_2} \mathcal{L} dt \quad (2-16)$$

where $\mathcal{L} = \mathcal{T} - \mathcal{U}$ is the Lagrangian of the system, and \mathcal{T}, \mathcal{U} are the kinetic and potential energy, respectively.

Hamilton's principle of least action states that the path a conservative mechanical system takes between two states \mathbf{x}_1 and \mathbf{x}_2 at time t_1 and t_2 , is the one for which Equation 2-16 is a stationary point, resulting in

$$\delta S = \int_{t_1}^{t_2} \delta \mathcal{L} dt = 0 \quad (2-17)$$

where $\delta\mathcal{L}$ is the variation of the Lagrangian. For systems with non-conservative forces and moments, Equation 2-17 is extended to

$$\delta S = \int_{t_1}^{t_2} (\delta W + \delta\mathcal{L}) dt = 0 \quad (2-18)$$

where δW is the virtual work. Equation 2-18 is applied to the QR-Load system, where the configuration manifold is $\mathbb{R}^3 \times \mathbb{S}^2 \times SO(3)$. With the following states

$$\mathbf{x} = [x_L \quad \dot{x}_L \quad q \quad \omega \quad R \quad \Omega]^T \quad (2-19)$$

The kinetic energy \mathcal{T} and the potential energy \mathcal{U} for the system are denoted as

$$\begin{aligned} \mathcal{T} &= \frac{1}{2} m_Q \dot{x}_Q \cdot \dot{x}_Q + \frac{1}{2} m_L \dot{x}_L \cdot \dot{x}_L + \frac{1}{2} \Omega \cdot J \cdot \Omega \\ \mathcal{U} &= m_Q g x_Q \cdot e_3 + m_L g x_L \cdot e_3 \end{aligned} \quad (2-20)$$

where $J \in \mathbb{R}^{3 \times 3}$ is the inertia tensor of the QR, and g is the gravity constant.

The energy can be rewritten in terms of q and x_L , by substituting Equation 2-14, giving

$$\mathcal{T} = \frac{1}{2} (m_Q + m_L) \dot{x}_L \cdot \dot{x}_L - m_Q L \dot{x}_L \cdot \dot{q} + \frac{1}{2} m_Q L^2 \dot{q} \cdot \dot{q} + \frac{1}{2} \Omega \cdot J \cdot \Omega \quad (2-21)$$

$$\mathcal{U} = (m_Q + m_L) g x_L \cdot e_3 - m_Q g L q \cdot e_3 \quad (2-22)$$

Variations The variations of \mathcal{T} and \mathcal{U} are approximated by a first-order Taylor approximation, which results in

$$\begin{aligned} \delta\mathcal{T} &\approx \frac{\partial\mathcal{T}}{\partial\dot{x}_L} \delta\dot{x}_L + \frac{\partial\mathcal{T}}{\partial\dot{q}} \delta\dot{q} + \frac{\partial\mathcal{T}}{\partial\Omega} \delta\Omega \\ &= ((m_Q + m_L) \dot{x}_L - m_Q L \dot{q}) \cdot \delta\dot{x}_L + (-m_Q L \dot{x}_L + m_Q L^2 \dot{q}) \cdot \delta\dot{q} + (J\Omega) \cdot \delta\Omega \\ \delta\mathcal{U} &\approx \frac{\partial\mathcal{U}}{\partial x_L} \delta x_L + \frac{\partial\mathcal{U}}{\partial q} \delta q \\ &= ((m_Q + m_L) g e_3) \cdot \delta x_L - (m_Q g L e_3) \cdot \delta q \end{aligned} \quad (2-23)$$

The first term of virtual work is obtained from f acting on the QR and is given by the following term,

$$\begin{aligned} \delta W_1 &= f R e_3 \cdot \sum_{j=1}^3 \frac{\partial x_Q}{\partial \mathbf{q}_j} \delta \mathbf{q}_j \\ &= f R e_3 \cdot (\delta x_L - L \delta q) \end{aligned} \quad (2-24)$$

where $\mathbf{q}_j = x_L, q, R$ and x_Q is substituted by Equation 2-14. The second term of virtual work is obtained from M acting on the QR. This gives the following term

$$\begin{aligned} \delta W_2 &= M \cdot \sum_{j=1}^3 \frac{\partial \Omega}{\partial \dot{\mathbf{q}}_j} \delta \dot{\mathbf{q}}_j \\ &= M \cdot (R^T \delta R) \end{aligned} \quad (2-25)$$

The variations in energy and the virtual work can be substituted into Equation 2-18, such that

$$\delta S = \int_{t_1}^{t_2} (\delta W_1 + \delta W_2 + \delta \mathcal{T} - \delta \mathcal{U}) dt \quad (2-26)$$

While x_L, \dot{x}_L vary on \mathbb{R}^3 , Equation 2-26 is also a function of variations on manifolds, where δR is a variation on $SO(3)$ and δq is a variation on \mathbb{S}^2 . These so called infinitesimal variations are obtained required as shown in [11, 13, 14, 15].

$$\begin{aligned} \delta R &= R\hat{\eta} \in T_R SO(3) \quad , \text{ where } \eta \in \mathbb{R}^3, \hat{\eta} \in \mathfrak{so}(3) \\ \delta q &= \xi \times q \in T_q \mathbb{S}^2 \quad , \text{ where } \xi \in \mathbb{R}^3, \xi \cdot q = 0 \end{aligned} \quad (2-27)$$

The following variations follow from differentiation,

$$\begin{aligned} \delta \dot{q} &= \dot{\xi} \times q + \xi \times \dot{q}, \\ \delta \dot{R} &= \dot{R}\hat{\eta} + R\dot{\hat{\eta}}, \\ \delta \hat{\Omega} &= \delta(R^T \dot{R}) \\ &= \delta R^T \dot{R} + R^T \delta \dot{R} \\ &= (R\hat{\eta})^T \dot{R} + R^T (\dot{R}\hat{\eta} + R\dot{\hat{\eta}}) \\ &= \hat{\eta}^T \hat{\Omega} + \hat{\Omega} \hat{\eta} + \dot{\hat{\eta}} \\ &= (\hat{\Omega} \eta)^\wedge + \dot{\hat{\eta}}, \\ \delta \Omega &= (\hat{\Omega} \eta) + \dot{\hat{\eta}} \end{aligned} \quad (2-28)$$

These variations are substituted into Equation 2-26, allowing it to be a function of variations in each generalized coordinate.

$$\begin{aligned} \delta S &= \int_{t_1}^{t_2} (\delta W_1 + \delta W_2 + \delta \mathcal{T} - \delta \mathcal{U}) dt \\ &= \int_{t_1}^{t_2} (((m_Q + m_L)\dot{x}_L - m_Q L\dot{q}) \cdot \delta \dot{x}_L + (fRe_3 - (m_Q + m_L)ge_3) \cdot \delta x_L) dt \\ &\quad \int_{t_1}^{t_2} ((m_Q L^2 \dot{q} - m_Q L\dot{x}_L) \cdot \delta \dot{q} + (m_Q gLe_3 - fLRe_3) \cdot \delta q) dt \\ &\quad \int_{t_1}^{t_2} (\Omega^T J \cdot \delta \Omega + M \cdot (R^T \delta R)) dt \end{aligned} \quad (2-29)$$

After rearranging and setting each variation to 0, the following equations of motion for the QR-Load system are found. Where, Equations 2-35 and 2-34

$$\frac{d}{dt} x_L = \dot{x}_L \quad (2-30)$$

$$(m_Q + m_L)(\ddot{x}_L + ge_3) = (q \cdot fRe_3 - m_Q L(\dot{q} \cdot \dot{q}))q \quad (2-31)$$

$$\dot{q} = \omega \times q \quad (2-32)$$

$$m_Q L\dot{\omega} = -q \times fRe_3 \quad (2-33)$$

$$\dot{R} = R\hat{\Omega} \quad (2-34)$$

$$J\dot{\Omega} + \Omega \times J\Omega = M \quad (2-35)$$

Summary

In this chapter, the dynamical model of the Quadrotor-Load system was derived. The motivation to use Geometric Mechanics and a basic understanding of its concepts are given in order to understand the difference between a Nonlinear Geometric model and a model obtained with classical modeling approaches.

With the tools of differential geometry, the system dynamics are expressed on nonlinear configuration manifolds, which results in a globally defined, compact, unambiguous representation of the model. This dynamical model is used for a nonlinear geometric control approach, which is discussed in the next chapter.

Chapter 3

Control Design

Section 3-1 introduces the concepts of Nonlinear Geometric Control, and the control design structure is discussed. The required control inputs are calculated by defining the tracking errors on nonlinear manifolds similar to the representation of the system dynamics.

Different flight are necessary to control the under-actuated system. A backstepping control approach is applied for the control of the load position tracking problem, allowing different controllers to operate in a cascaded structure. The controllers that are designed for each flight mode, are discussed in Sections 3-2, 3-3 and 3-4.

bart: Descibe just as in chapter 2 what we are going to read in the next sections

nam: please check

3-1 Nonlinear Geometric Control

Many control systems are developed for the standard form of ordinary differential equations, namely $\dot{x} = f(x, u)$, where the state and the control input are denoted by x and u . It is assumed that the state and the control input lie in Euclidean spaces, and the system equations are defined in terms of smooth functions between Euclidean spaces. However, for many mechanical systems, the configuration space can only be expressed locally as Euclidean space. In order to express the configuration space globally, a nonlinear space is required.

Geometric Control Theory is the study on how geometry of the state space influences controls problems. In control systems engineering, the underlying geometric features of a dynamic system are often not considered carefully. Differential geometric control techniques utilize these geometric properties for control system design and analysis. The objective is to express the system dynamics and control inputs on manifolds instead of local charts. In contrast to locally

defined linear control, nonlinear geometric control can be defined almost globally, avoiding singularities that occur in the representation of large angles and complex maneuvering.

Global nonlinear dynamics of various classes of closed loop attitude control systems have been studied in recent years [16]. In contrast to hybrid control systems [17], complicated reachability set analysis is not required to guarantee safe switching between different flight modes, as the region of attraction for each flight mode covers the configuration space almost globally.

Backstepping Control A backstepping approach, or cascade control, is a Lyapunov based technique to design the control of nonlinear dynamical systems and ensuring Lyapunov stability. This approach is commonly used for the control of QRs [18] and will also be used in this research for the control of the load trajectory tracking problem.

The basic principle is to create a cascaded structure by starting with a stable system as a base, then "stepping back" from this base to add a control loop around it that stabilizes the added subsystem to enable the control of another state. This is repeated until the final external control is reached, see Figure 3-1. The control law is designed by using states as virtual control signals. Each loop computes a virtual command signal for an inner loop, denoted by q_c and R_c , being the computed load attitude and QR attitude, respectively.

Because the QR has only four actuators, it is not possible to control all DOFs of the QR-Load system simultaneously. The backstepping approach allows control of different flight modes in which parts of the DOFs are controlled. The flight modes and their functions are defined in order, from the most inner loop to the most outer loop, as follows

- QR Attitude Controlled Mode
 - Track a desired QR attitude $R_d(t)$ and a heading direction $b_{1d}(t)$
 - Give a desired input M for system
- Load Attitude Controlled Mode
 - Track a desired load attitude command $q_d(t)$
 - Give a computed QR attitude R_c for the QR attitude controller (instead of $R_d(t)$)
- Load Position Controlled Mode
 - Track a desired load position $x_{L,d}(t)$
 - Give a computed load attitude q_c for the load attitude controller (instead of $qR_d(t)$)

where the subscript d denotes a desired tracking reference, and the subscript c denotes a computed value that is calculated as a tracking reference. The difference in this notation is whether the signal is a predefined desired signal, or a signal computed by a controller.

The controller that is used in this research is shown in Figure 3-1. The lowest levels have the highest bandwidth and are in control of the rotor rotational speeds ω_i , the total force f and moments M . The next level controls the load attitude q , and the top level controls the load position x_L .

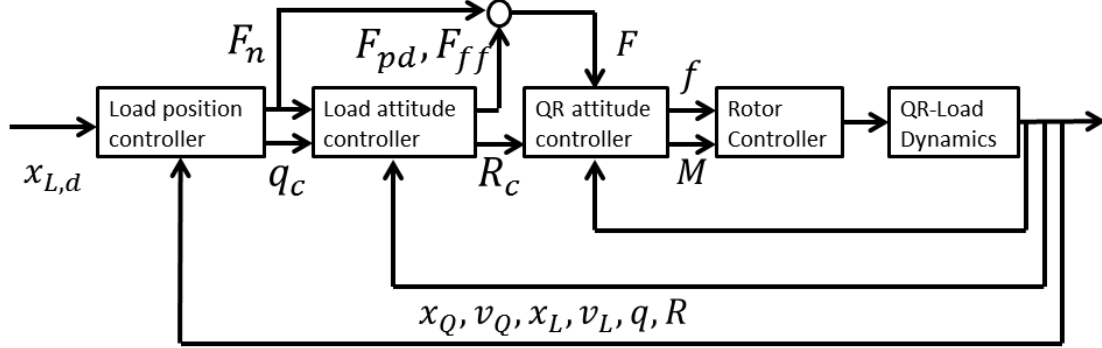


Figure 3-1: Nonlinear Geometric Control Loop of the QR-Load system [15]

The design of the controllers for the QR attitude can be found in [3] and for the load attitude- and position this can be found in [15]. Thorough stability analyses are presented in either references. For a deeper understanding of Lyapunov stability analysis in geometric control, the reader can refer to [14].

Configuration Errors The system dynamics evolve on nonlinear manifolds that describe the configuration spaces for the QR attitude $\in SO(3)$ and the load attitude $\in \mathbb{S}^2$. Likewise, configuration errors can be described on these manifolds. The derivation of the attitude and velocity errors can be found in [14].

Recall that R is the rotation matrix for the QR attitude, and R_d is the desired rotation matrix. Then, the attitude error is denoted as $R_d^T R$, and describes the relative rotation from the body frame to the desired frame. The QR attitude error function on $SO(3)$ is chosen to be

$$\Psi_R(R, R_d) = \frac{1}{2} \text{tr} [I - R_d^T R] \quad (3-1)$$

Ψ_R is locally positive-definite about $R_d^T R = I$ within the region where the rotation angle between R and R_d is less than 180° . It can be shown that this region where $\Psi_R < 2$ almost covers $SO(3)$. The derivative of Equation 3-1 is given by

$$\mathbf{D}_R \Psi(R, R_d) \cdot R \hat{\eta} = \frac{1}{2} (R_d^T R - R^T R_d)^\vee \cdot \eta \quad (3-2)$$

where the *vee map* $^\vee : \mathfrak{so}(3) \rightarrow \mathbb{R}^3$ is the inverse of the *hat map* defined in Section 2-1. Equation 2-27 states that the variation of the rotation matrix is expressed as $\delta R = R \hat{\eta}$ for $\eta \in \mathbb{R}^3$. From this derivative, the attitude tracking error is obtained

$$e_R = \frac{1}{2} (R_d^T R - R^T R_d)^\vee \quad (3-3)$$

It is important to note that the tangent vectors \dot{R} and \dot{R}_d cannot be compared directly, since they do not lie in the same space. \dot{R} and \dot{R}_d are expressed in their own tangent spaces, denoted by $T_R SO(3)$ and $T_{R_d} SO(3)$, respectively.

\dot{R}_d is transformed into a vector on $T_R SO(3)$ to compare it with \dot{R} . This is done by a mathematical object called a *transport map*, which enables the comparison of tangent vectors living in different spaces. See Figure 3-2, where two curves $R(t), R_d(t)$ evolve on manifold $SO(3)$. Transport map $\mathcal{T}(R, R_d) : T_{R_d} SO(3) \mapsto T_R SO(3)$ allows comparison of the two tangent vectors.

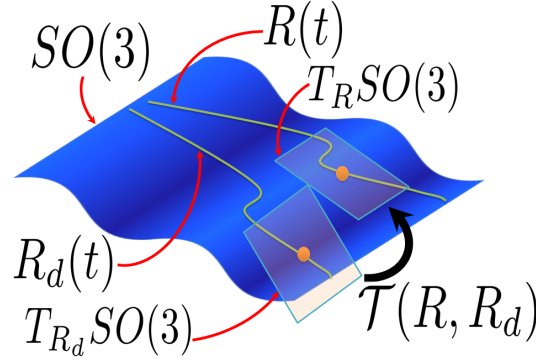


Figure 3-2: Transport map $\mathcal{T}(R, R_d)$

The velocity error that corresponds to the transport map $\mathcal{T}(R, R_d)$ is defined as

$$\dot{e} = \dot{R} - \dot{R}_d(R_d^T R) \quad (3-4)$$

This can be rewritten as follows

$$\begin{aligned} \dot{R} - \dot{R}_d(R_d^T R) &= R\hat{\Omega} - R_d\hat{\Omega}_d(R_d^T R) \\ &= R(\Omega)^\wedge - (RR^T)R_d\hat{\Omega}_dR_d^T R \\ &= R(\Omega)^\wedge - R(R^T R_d\Omega_d)^\wedge \\ &= R(\Omega - R^T R_d\Omega_d)^\wedge \end{aligned} \quad (3-5)$$

From this follows that the velocity tracking error e_Ω in $\{\mathcal{B}\}$ is defined as

$$e_\Omega = \Omega - R^T R_d\Omega_d \quad (3-6)$$

Next, the load attitude error function on \mathbb{S}^2 represents the distance from the direction q to the desired direction q_d , and is given by

$$\Psi_q = 1 - q_d^T q \quad (3-7)$$

In the same fashion a *transport map* is used for a comparison between the tangent spaces $T_q \mathbb{S}^2$ and $T_{q_d} \mathbb{S}^2$. This results in the following error functions on $T\mathbb{S}^2$

$$e_q = \hat{q}^2 q_d \quad (3-8)$$

$$e_{\dot{q}} = \dot{q} - (q_d \times \dot{q}_d) \times q \quad (3-9)$$

The tracking errors for position and velocity are defined as

$$e_x = x - x_d \quad (3-10)$$

$$e_v = v - v_d \quad (3-11)$$

where $v_d = \dot{x}_d$ and $x_d(t) \in \mathbb{R}^3$ is a smooth desired load position.

3-2 Quadrotor Attitude Tracking

The QR Attitude Controlled Mode is designed to control the QR attitude by tracking a smooth desired QR attitude command $R_d(t)$. This is done by controlling the error dynamics of e_R and e_Ω . The derivations of the equations in this section can be found in Section A-4. From Equations 3-3 and 3-6, the derivative of the attitude tracking error e_R can be written as

$$\dot{e}_R = \frac{1}{2}(R_d^T R \hat{e}_\Omega + \hat{e}_\Omega R^T R_d)^\vee \quad (3-12)$$

It can be shown that $\|\dot{e}_R\| \leq \|e_\Omega\|$ for all $R_d^T R \in SO(3)$.

From Equations 2-34, 2-35 and 3-6, follow that the derivative of the angular velocity tracking error e_Ω can be written as

$$\dot{e}_\Omega = J^{-1}(-\Omega \times J\Omega + M) + \hat{\Omega} R^T R_d \Omega_d - R^T R_d \dot{\Omega}_d \quad (3-13)$$

From Equation 2-34 follows that the kinematics equation for the attitude command can be written as

$$\dot{R}_d = R_d \hat{\Omega}_d \quad (3-14)$$

Which defines the desired angular velocity $\dot{\Omega}_d$ as follows

$$\begin{aligned} \hat{\Omega}_d &= R_d^T \dot{R}_d, \\ \dot{\hat{\Omega}}_d &= (\dot{R}_d^T \dot{R}_d) + (R_d^T \ddot{R}_d) \\ &= (R_d \hat{\Omega}_d)^T (R_d \hat{\Omega}_d) + (R_d^T \ddot{R}_d) \\ &= -\hat{\Omega}_d \hat{\Omega}_d + R_d^T \ddot{R}_d, \\ \dot{\Omega}_d &= (-\hat{\Omega}_d \hat{\Omega}_d + R_d^T \ddot{R}_d)^\vee \end{aligned} \quad (3-15)$$

Now the control input M can be defined as a proportional term, a derivative term and a canceling term, as follows [15]

$$M = -\frac{1}{\epsilon^2} k_R e_R - \frac{1}{\epsilon} k_\Omega e_\Omega + \Omega \times J\Omega - J(\hat{\Omega} R^T R_d \Omega_d - R^T R_d \dot{\Omega}_d) \quad (3-16)$$

for any positive constants k_R, k_Ω , and $0 < \epsilon < 1$. Where ϵ is a parameter to enable rapid exponential convergence of the attitude- and angular velocity error functions.

With this control input Equation 3-13 is reduced to

$$J\dot{e}_\Omega = -\frac{1}{\epsilon^2} k_R e_R - \frac{1}{\epsilon} k_\Omega e_\Omega \quad (3-17)$$

A stability analysis of the controller is presented in [3] and it is proven that the zero equilibrium of the closed loop tracking error $(e_R, e_\Omega) = (0, 0)$ is exponentially stable, if the initial conditions satisfy

$$\Psi_R(R(0), R_d(0)) < 2 \quad (3-18)$$

$$\|e_\Omega(0)\|^2 < \frac{2}{\lambda_M(J)} \frac{k_R}{\epsilon^2} (2 - \Psi_R(R(0), R_d(0))) \quad (3-19)$$

where $\lambda_M(\cdot)$ denotes the maximum eigenvalue. The domain of attraction is defined by Equations 3-18 and 3-19.

Furthermore, there exist constants $\alpha_R, \beta_R > 0$ such that

$$\Psi_R(R(t), R_d(t)) \leq \min \left\{ 2, \alpha_R e^{-\beta_R t} \right\} \quad (3-20)$$

3-3 Load Attitude Tracking

The Load Attitude Controlled Mode tracks a desired load attitude q_d by calculating a command signal for the QR attitude, defined as

$$R_c = [b_{1c}; b_{3c} \times b_{1c}; b_{3c}] \quad (3-21)$$

where $b_{3c} \in \mathbb{S}^2$ is defined by

$$b_{3c} = \frac{F}{\|F\|} \quad (3-22)$$

Such that F in Equation 3-22 is defined by a normal component F_n , F_{pd} and F_{ff}

$$F = F_n - F_{pd} - F_{ff} \quad (3-23)$$

Control forces for a system evolving on \mathbb{S}^2 , are derived in [14]. This results in a proportional-derivative force F_{pd} and a feed forward force F_{ff} , that are functions of Equations 3-8 and 3-9. The following terms are obtained

$$\begin{aligned} F_{pd} &= -k_P \hat{q}^2 q_d - k_D (\dot{q} - (q_d \times \dot{q}_d \times q)) \\ &= -k_q e_q - k_\omega e_{\dot{q}} \end{aligned} \quad (3-24)$$

$$F_{ff} = m_Q L \langle \langle q, q_d \times \dot{q}_d \rangle \rangle_{\mathbb{R}^3} (q \times \dot{q}) + m_Q L (q_d \times \ddot{q}_d) \times q \quad (3-25)$$

The unit vector b_{1c} is defined as

$$b_{1c} = -\frac{1}{\|b_{3c} \times b_{1d}\|} (b_{3c} \times (b_{3c} \times b_{1d})) \quad (3-26)$$

where $b_{1d} \in \mathbb{S}^2$ is chosen, not parallel to b_{3c} . The total upward thrust is defined as

$$f = F \cdot R e_3 \quad (3-27)$$

It is proven in [15] that the zero equilibrium of the closed loop tracking error $(e_q, e_{\dot{q}}, e_R, e_\Omega) = (0, 0, 0, 0)$ is exponentially stable, if the initial conditions satisfy

$$\Psi_q(q(0), q_d(0)) < 2 \quad (3-28)$$

$$\|e_{\dot{q}}(0)\|^2 < \frac{2}{m_Q L} k_R (2 - \Psi_q(q(0), q_d(0))) \quad (3-29)$$

The domain of attraction is defined by Equations 3-18, 3-19, 3-28 and 3-29. Furthermore, there exist constants $\alpha_q, \beta_q > 0$ such that

$$\Psi_q(q(t), q_d(t)) \leq \min \left\{ 2, \alpha_q e^{-\beta_q t} \right\} \quad (3-30)$$

3-4 Load Position Tracking

Tracks load position reference. Outputs load attitude reference.

$$q_c = -\frac{A}{\|A\|} \quad (3-31)$$

where

$$A = -k_x e_x - k_v e_v + (m_Q + m_L)(\ddot{x}_{L,d} + g e_3) + m_Q L(\dot{q} \cdot \dot{q})q \quad (3-32)$$

with $e_x = x_L - x_{L,d}$ and $e_v = \dot{x}_L - \dot{x}_{L,d}$. Furthermore, F_n is redefined as

$$F_n = (A \cdot q)q \quad (3-33)$$

It is proven in [15] that the zero equilibrium of the closed loop tracking error $(e_x, e_v, e_q, e_{\dot{q}}, e_R, e_{\Omega}) = (0, 0, 0, 0, 0, 0)$ is exponentially stable, if the initial conditions satisfy

$$\Psi_q(q(0), q_c(0)) < \psi_1 < 1 \quad (3-34)$$

$$\|e_x(0)\|^2 < e_{x_{max}} \quad (3-35)$$

where $e_{x_{max}}$ and ψ_1 are fixed design depended constants.

The domain of attraction is defined by Equations 3-18, 3-19, 3-34 and the following equation

$$\|e_{\dot{q}}(0)\|^2 < \frac{2}{m_Q L} k_q (\psi_1 - \Psi_q(q(0), q_d(0))) \quad (3-36)$$

Furthermore, there exist constants $\alpha_q, \beta_q > 0$ such that

$$\Psi_q(q(t), q_d(t)) \leq \min \left\{ 2, \alpha_q e^{-\beta_q t} \right\} \quad (3-37)$$

3-5 Stability Analysis

Normally Lyapunov Analysis is

Lyapunov Analysis on $SO(3) \times R^3$ and $S^2 \times R^3$ Closed-loop full-attitude dynamics evolve on the non- Euclidean manifold $SO(3) \times R^3$. Since these manifolds are locally Euclidean, local stability properties of a closed-loop equilibrium solution can be assessed using standard Lyapunov methods. In addition, the LaSalle invariance result and related Lyapunov results apply to closed-loop vector fields defined on these manifolds. However, since the manifolds $SO(3)$ and S^2 are compact, the radial unboundedness assumption cannot be satisfied; consequently, global asymptotic stability cannot follow from a Lyapunov analysis on Euclidean spaces [40], and therefore must be analyzed in alternative ways [19]–[23]. [8, p.43]

[8] summarizes global results on attitude control and stabilization for a rigid body using continuous time- invariant feedback. The analysis uses methods of geometric mechanics based on the geometry of the special orthogonal group $SO(3)$ and the two-sphere S^2 .

Bart: Ok, but what are you doing with this? Does this relate to backstepping?

Bart: Does this include a part about tuning of the controller?

Summary

In this chapter the control design based on Nonlinear Geometric Control was discussed.

The main difference with other control techniques is that the tracking errors are also defined on manifolds, which allows the design of almost global defined controllers.

Stability analysis is different from a Lyapunov analysis on Euclidean spaces.

In order to test the control performance of a load position tracking objective, experiments are defined in the next chapter.

Chapter 4

Experiment

The experimental procedure is explained in Section 4-1. It is discussed what experiments can be done in order to investigate the potential of nonlinear geometric control. In addition a comparison will be made between the performances of the Nonlinear Geometric Controller and a linear LQR controller.

The controllers are tested on their ability to track a desired load trajectory. Section 4-2 presents trajectories that create situations with different challenges. It is discussed what could be expected from these experiments, and the differences in performance of the controllers is discussed.

In Section 4-3 the experimental setup is discussed. The model parameters for the QR-Load system are presented, as well as the controller parameters for both nonlinear Geometric controller and LQR controller. The notion of a backstepping command filter is made to explain a mathematical simplification in the experiments.

4-1 Procedure

Performance of both LQR control and a Nonlinear Geometric Control could be evaluated by comparing their ability to track a load trajectory with minimal error. In linear control however, a linearized model is obtained by assuming small angles of both load and QR around an equilibrium point. The load position is defined as the position, a cable length underneath the QR position. This makes the model over-defined if the load position is included. As a result, the linearized model does not allow direct reference tracking of the load position.

The LQR cost function allows control of the inputs f and M , and the states which define the QR position, QR attitude and load attitude. Therefore, load control is only possible in means of minimizing the load swing. This fact illustrates an important difference between the use of a linear and a nonlinear model.

The experiments describe a desired load trajectory $x_{L,d}(t)$, which is required to be smooth for Geometric Control, such that feed forward terms can be generated and implemented. In this

thesis the desired load paths are generated by hand, and the required velocity and acceleration is calculated by a command filter, of which the details are described in Section 4-3.

The experiments done with the LQR controller will apply reference tracking of the QR position, which is based on the desired load trajectories that are used for the nonlinear Geometric controller. When assuming small angles and minimal load swing, the QR position is approximately a cable length above the predefined desired load position. Note that this will not allow a direct comparison of the load trajectory tracking, nevertheless this will illustrate the main differences between the controllers with the same purpose of load transportation, but with a different approach.

4-2 Trajectories

What observations can be made in order to adapt the controller properties that improve performance of the test cases. Description of tests that apply on all cases.

4-2-1 Case A

In this case a smooth step-like trajectory is generated to transport the load from a starting position along the direction of the x-axis to the final position. In a regular step function the system is subjected to a sudden input. The stability of the system can be investigated by observing whether it is able to reach a stationary final state, and how fast this can be reached. It can be seen whether the system responds with an overshoot and how fast the response is, when the controller tries to track the trajectory.

Figure 4-1 shows the desired trajectory over time, and a three dimensional representation.

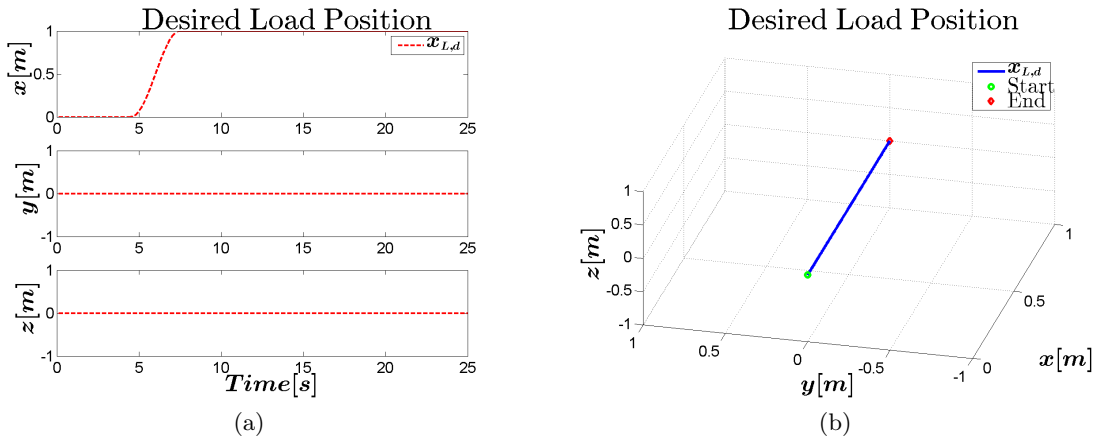


Figure 4-1: Desired Load Position Case A

4-2-2 Case B

PLANNING: make case to test limits on QR angles while tracking load trajectory. Is nonlinear GC useful for such aggressive maneuvers?

4-2-3 Case C

For this case a trajectory is generated to test multiple disciplines. The trajectory has the shape of a sine wave that moves along the y-axis and varies in amplitude in the direction of the x-axis, while going up and down in the direction of the z-axis. The changing amplitude of the trajectory that moves from side to side, requires varying velocities to 'keep up' with the trajectory. It can be expected that the nonlinear geometric control allows large **QR** angles, whereas the **LQR** will possibly fail to deviate far from the equilibrium point.

Figure 4-2 shows the desired trajectory over time, and a three dimensional representation.

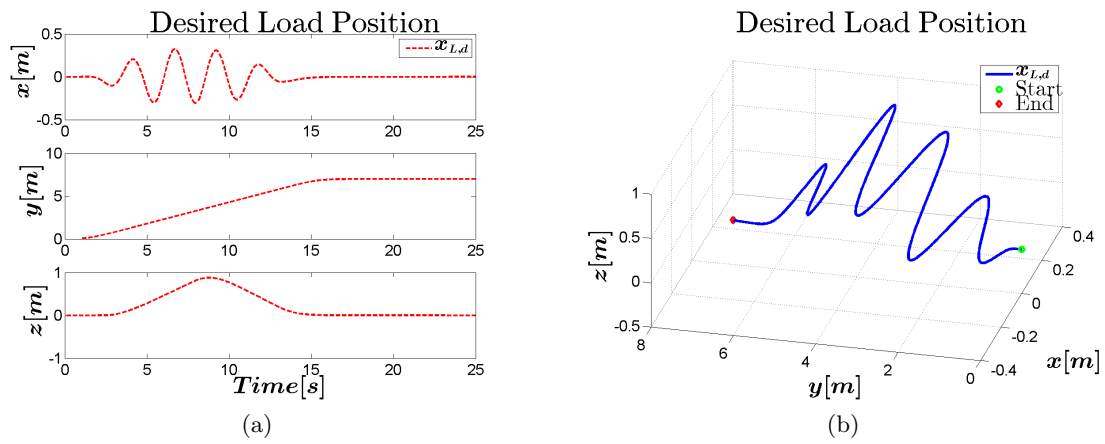


Figure 4-2: Desired Load Position Case C

4-3 Setup

Model parameters The simulations are developed using Matlab and Simulink, using the system parameters found in Table 4-1.

Parameter	Value	Description
m_Q	4.34 kg	Quadrotor Mass
m_L	0.1 kg	Load Mass
l	0.315 m	Arm length from QR com! to rotor
L	0.7 m	Cable Length
I_{xx}	0.0820 kgm^2	Quadrotor Inertia about x-axis
I_{yy}	0.0845 kgm^2	Quadrotor Inertia about y-axis
I_{zz}	0.1377 kgm^2	Quadrotor Inertia about z-axis
d		Drag Constant
b		Thrust Constant
c_{τ_f}		Constant

Table 4-1: Modeling Parameters

LQR Control Linear Quadratic Regulator (LQR) control uses an algorithm to obtain a state-feedback controller, minimizing a cost function depending on the states and weight factors. An LQR design is shown in Figure 4-3



Figure 4-3: LQR control design

LQR control is based on a small angle assumption. Therefore, a traditional modeling method may represent the rotation matrix with a local coordinate system, for example with an Euler Angle parameterization. A continuous time linearized model of the system used in this controller is represented in the following form

$$\dot{\mathbf{x}} = A\mathbf{x} + Bu \quad (4-1)$$

$$y = C\mathbf{x} + Du \quad (4-2)$$

where \mathbf{x} is the state vector and u is the input vector, defined as follows

$$\mathbf{x} = [x \ y \ z \ \phi \ \theta \ \psi \ \phi_L \ \theta_L \ \dot{x} \ \dot{y} \ \dot{z} \ \dot{\phi} \ \dot{\theta} \ \dot{\psi} \ \dot{\phi}_L \ \dot{\theta}_L]^T \quad (4-3)$$

$$u = [f \ M_\phi \ M_\theta \ M_\psi]^T \quad (4-4)$$

where ϕ_L and θ_L are the angle of rotation of the load about the x-axis and y-axis in $\{\mathcal{B}\}$, respectively. The derivation of A, B, C, D can be found in Section A-2.

Using Matlab command `lqr(A,B,Q,R)`, an optimal gain matrix K is calculated, such that the state-feedback law $u = -K\mathbf{x}$ minimizes the quadratic cost function defined as

$$J(u) = \int_0^\infty (\mathbf{x}^T Q \mathbf{x} + u^T R u) dt \quad (4-5)$$

The weight matrices Q and R that define the effects of the states and inputs in the cost function, and the calculated gain matrix K can be found in Section A-2.

Geometric Control The chosen controller gains in Equations 3-16,3-21,3-31 can be found in Table 4-2.

Command Filtering A consequence of a backstepping control approach, is that it also increases the order of the states. The inner control loops become a function of the commanded signals and their higher derivatives, which are generated by an outer loop. In the earlier presented control design, the load attitude controller generates a commanded QR attitude R_c and its derivative \dot{R}_c . In the same fashion, the load position controller generates a commanded load attitude q_c and its derivative \dot{q}_c . Instead of analytic differentiation of these terms, which can be tedious and require high computational costs, these values can be obtained with the use of a Command Filter, which is explained in more detail in [19].

Gain	Value
k_R	
k_Ω	
k_q	
k_ω	
k_x	
k_v	

Table 4-2: Controller Gains

The basic idea is that the command signal is pre-filtered by a low pass filter and generates an estimation of the derivatives of the commanded signal. In this thesis a backstepping command filter of third order is applied to compute $\dot{R}_c, \ddot{R}_c, \dot{q}_c, \ddot{q}_c$. The transfer function of the original commanded input signal X_c^o and the filtered output X_c has the form

$$\frac{X_c(s)}{X_c^o(s)} = H(s) = \frac{\omega_{n1}}{s + \omega_{n1}} \cdot \frac{\omega_{n2}^2}{s^2 + 2\zeta\omega_{n2}s + \omega_{n2}^2} \quad (4-6)$$

Where ζ is the damping ratio and ω_n the undamped natural frequency. See Figure ?? and A-2. The filter has the following state space representation

$$\dot{x}_1 = x_2 \quad (4-7)$$

$$\dot{x}_2 = x_3 \quad (4-8)$$

$$\dot{x}_3 = -(2\zeta\omega_{n2} + \omega_{n1})x_3 - (2\zeta\omega_{n1}\omega_{n2} + \omega_{n2}^2)x_2 - (\omega_{n1}\omega_{n2}^2)(x_1 - x_c^o) \quad (4-9)$$

where $x_1 = x_c$, $x_2 = \dot{x}_c$ and $x_3 = \ddot{x}_c$.

Chapter 5

Results

The sections in this chapter discuss the results that are obtained from the load trajectory tracking experiments.

In Figures 5-2, 5-4 and 5-6 the load tracking performance is shown for the Nonlinear Geometric Controller. From these figures the tracking errors of the QR attitude, load attitude and load position, and the stability of the tracking errors can be analyzed.

5-1 Case A

Figure 5-1a shows the load position along the desired load position $x_{L,d}$ for both control approaches.

Figure 5-1b shows the load position error for both control approaches.

Figure 5-1c shows the QR attitude with respect to $\{\mathcal{I}\}$.

In Figure 5-1d the load angle with respect to $\{\mathcal{B}\}$ is shown.

Observations:

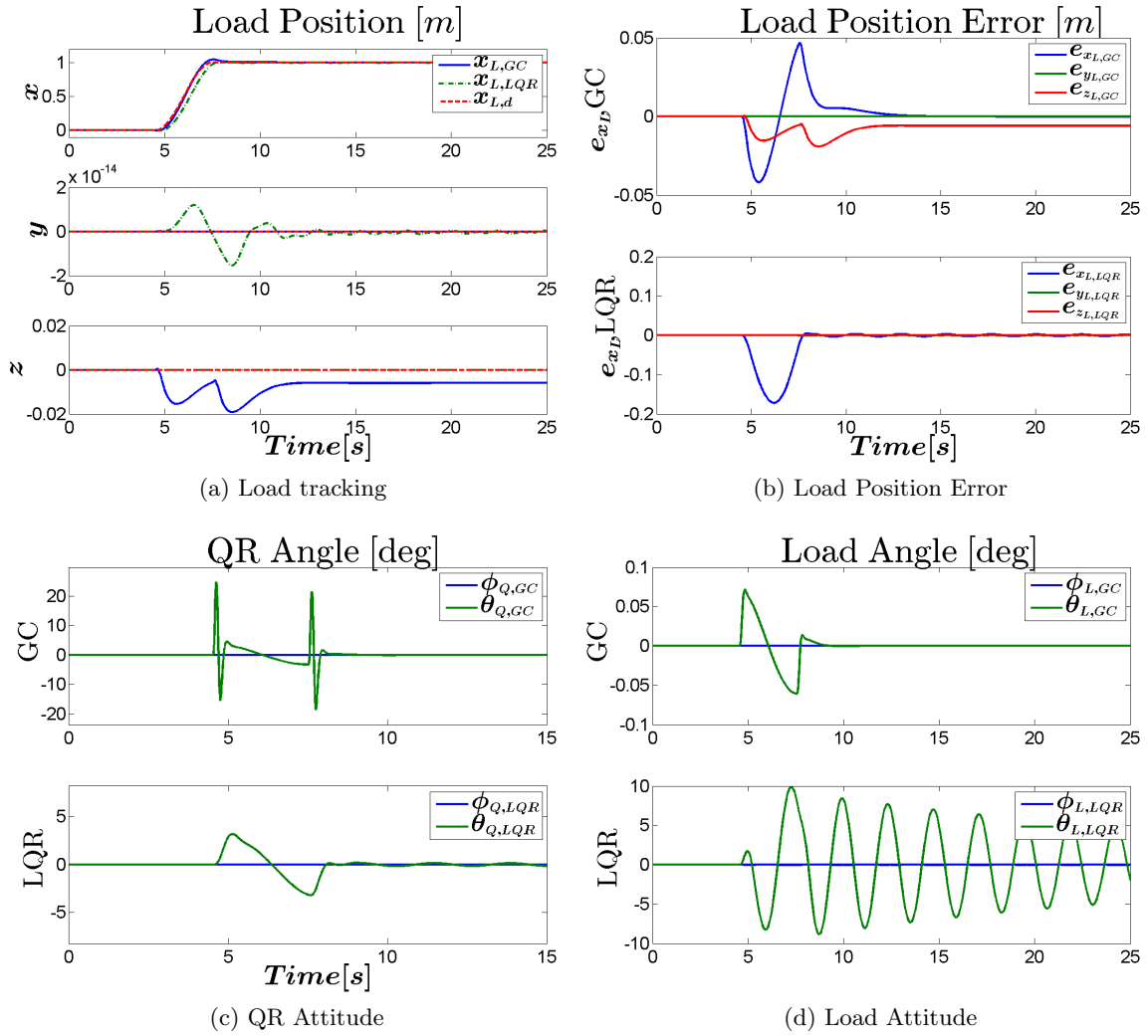


Figure 5-1: Controller Comparison Case A

The desired and actual load trajectory, and the position error are shown in Figure 5-2a and Figure 5-2b, respectively. From this can be seen that a small steady state error remains in the z-direction. However, $(e_x, e_y) = (0, 0)$ is exponentially attractive.

Figure 5-2c and 5-2d show the tracking errors of the QR attitude and load attitude, respectively.

Observations: $(e_x, e_v, e_q, e_{\dot{q}}, e_R, e_\Omega) = (0, 0, 0, 0, 0, 0)$ is exponentially stable

Figure 5-2e and 5-2f show the tracking error functions of the QR and load, respectively.

Observations: there exist constants $\alpha_q, \beta_q > 0$ such that

$$\Psi_q(q(t), q_d(t)) \leq \min \left\{ 2, \alpha_q e^{-\beta_q t} \right\} \quad (5-1)$$

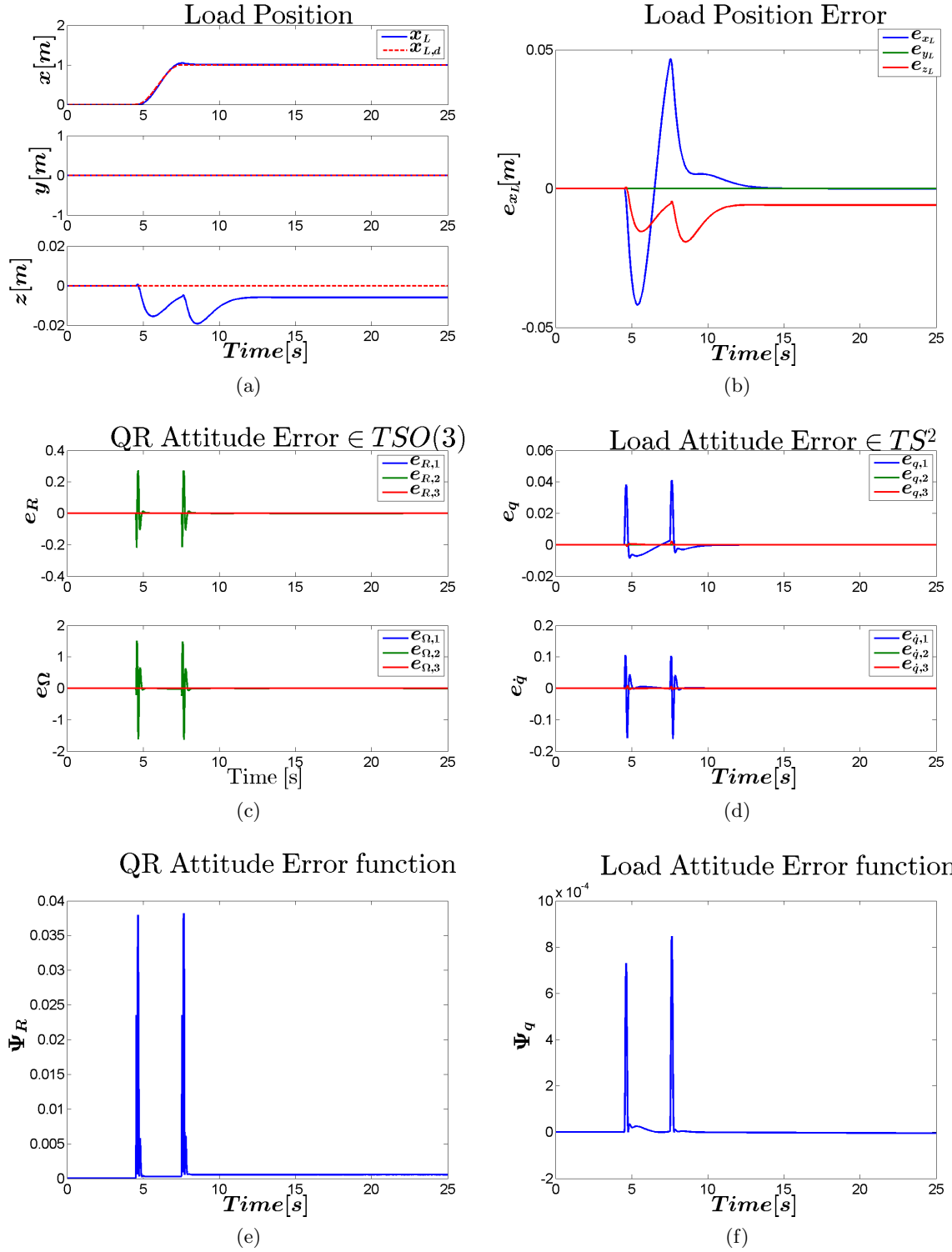


Figure 5-2: Results Nonlinear Geometric Control Case A

5-2 Case B

Figure 5-3a shows the load position along the desired load position $x_{L,d}$ of both controllers.



Figure 5-3: Controller Comparison Case B

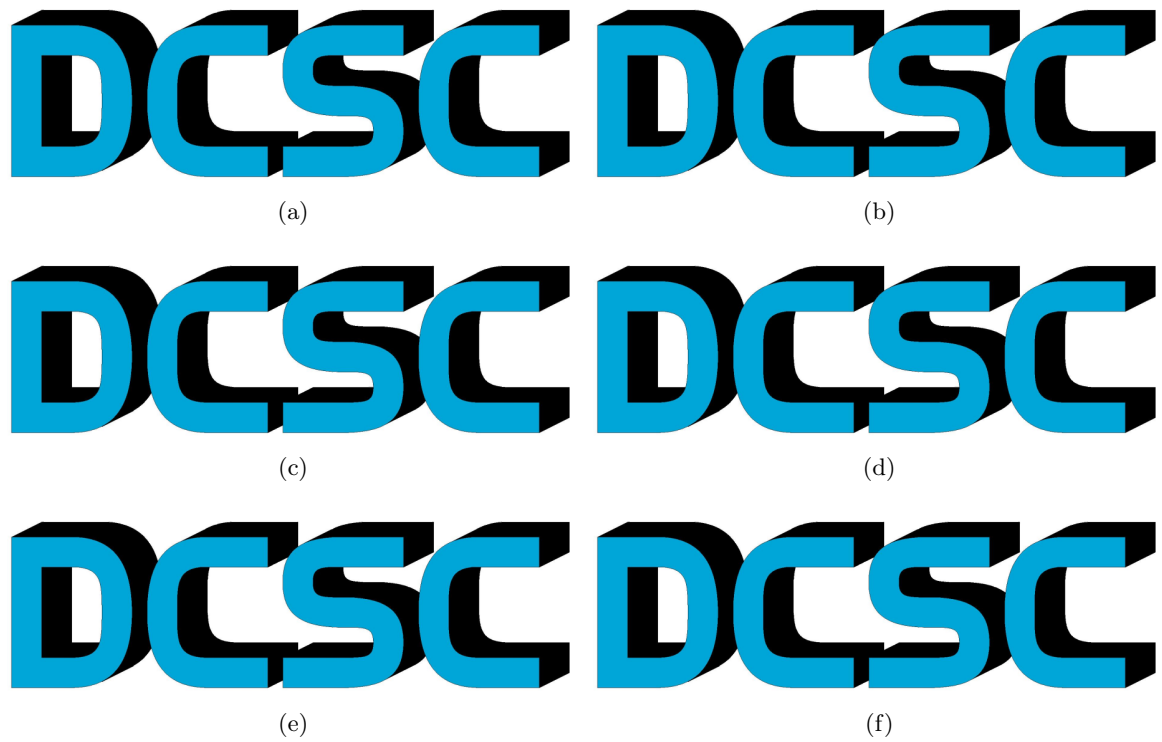


Figure 5-4: Results Nonlinear Geometric Control Case B

5-3 Case C

Figure 5-5a shows the load position along the desired load position $x_{L,d}$ of both controllers. Figure 5-5b shows the load position error for both control approaches.

Observations: fact that LQR can not control load position is obvious.

OTHER GAINS FOR LQR!

Very small penalty on load angle results in swinging load; decreasing load position error, but very bad anti-swing.

Figure 5-5c shows the QR attitude with respect to $\{\mathcal{I}\}$.

In Figure 5-5d the load angle with respect to $\{\mathcal{B}\}$ is shown.

Observations: Load angles are huge, check results

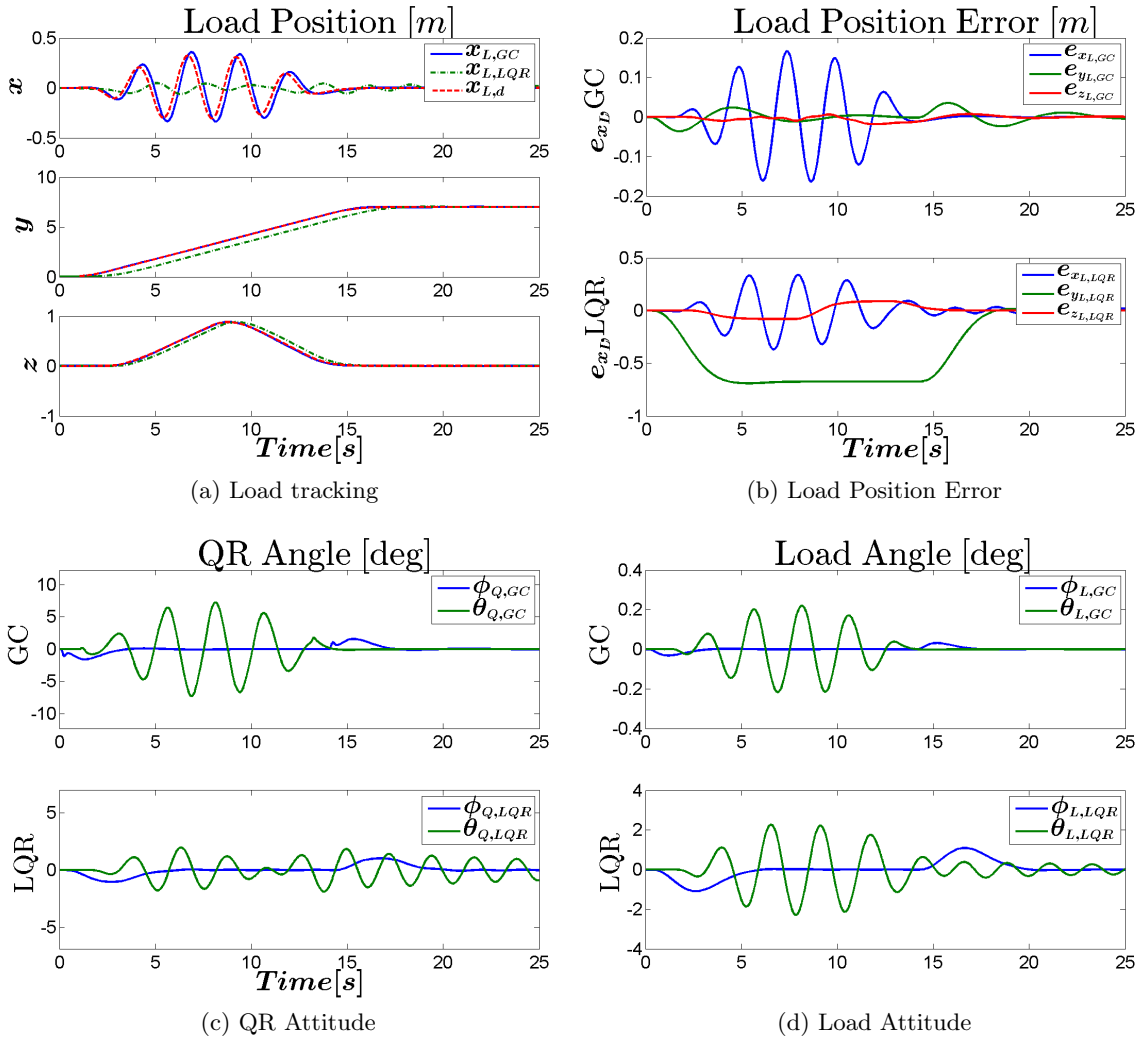


Figure 5-5: Controller Comparison Case C

While tracking the required QR attitude, which tilts the QR to reach the desired velocities in the right direction, it can be seen that the system has difficulties to also maintain the desired

height, which can be explained by the fact that the total force will not point upwards if the QR is tilted. Despite the fact that the QR is moving from side to side, the upward force is still controlled to track the desired height.

Figure 5-6a shows the desired load position, and Figure 5-6b shows that the error is mainly the overshoot in the x-direction, due to the fast desired swinging motion.

Figure 5-6c and 5-6d show the tracking errors of the QR attitude and load attitude, respectively.

Observations: $(e_x, e_v, e_q, e_{\dot{q}}, e_R, e_{\Omega}) = (0, 0, 0, 0, 0, 0)$ is exponentially stable

Figure 5-6e and 5-6f show the tracking error functions of the QR and load, respectively.

Observations: there exist constants $\alpha_q, \beta_q > 0$ such that

$$\Psi_q(q(t), q_d(t)) \leq \min \left\{ 2, \alpha_q e^{-\beta_q t} \right\} \quad (5-2)$$

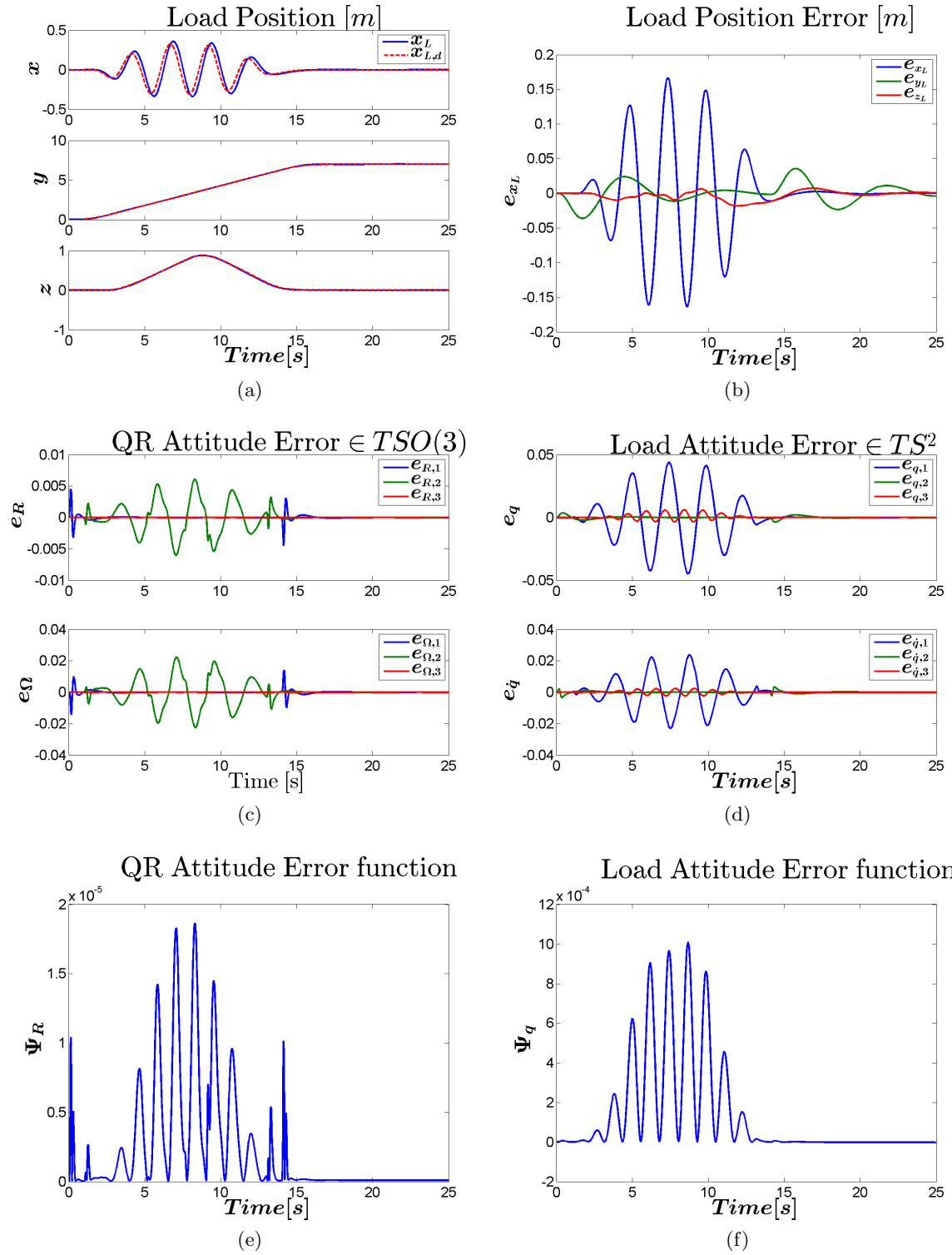


Figure 5-6: Results Nonlinear Geometric Control Case C

5-4 Conclusion

Near the equilibrium configuration, the **LQR** controller is able to reduce the swing.

The nonlinear geometric controller depends on feed forward terms that are obtained from the desired trajectories. Trajectory generation approaches exist that are able to generate the required desired position, velocity and acceleration by however it is possible to compute these with trajectory generating algorithms too.

The controllers are functions of the computed tracking references q_c, R_c and their derivatives. These terms are approximated by a command filter, which means that the accuracy decreases because high frequency terms are filtered.

Conclusions and Future Work

6-1 Summary and Conclusions

This report starts by introducing the subject. The aim is described and the motivation for this research is given.

After the main introduction, the concepts of Geometric Mechanics are introduced. Instead of the trivial Euclidean spaces defined by Cartesian coordinates, the configuration space of the model is described on nonlinear manifolds. This approach is used to obtain a model through the tools of Differential Geometry.

Based on the geometric model, a nonlinear geometric control design is discussed. A back-stepping approach, allows different **DOFs** of the under-actuated system to be controlled in a cascaded structure. The geometric control is based on are functions of error functions defined on nonlinear manifolds. by Differential Geometry.

Next, the experiment is defined. The nonlinear controller is used to track desired load trajectories in different situations. The nonlinear performance is compared to an **LQR** control Testing the nonlinear Geometric Controller To compare with a common linear controller, **LQR** control is used to compare Results are,

The conclusions that can be extracted from the experiments is that

6-2 Recommendations for Future Work

6-2-1 Investigate Implementation

Digital Control The concept of Geometric Control is shown under the assumption of continuous-time control. However, an analysis must be done in the discrete-time domain for the implementation of a real-time application. This must verify whether it is feasible to run the controller on an on-board processor on a **QR**. The control performance could be limited by the bandwidth of either the discretized control system or the wireless communication.

It must be investigated whether the control system is still able to deal with the fast dynamics that are required for aggressive maneuvering. Continuous-time Euler-Lagrange equations could be found by minimizing the action integral, which is a function of the Lagrangian. In a similar procedure the discrete-time Euler-Lagrange can be obtained, by minimizing the summation of a discrete Lagrangian, which is demonstrated in [10].

Model identification and validation In this thesis the model parameters are either obtained from examples in literature or arbitrarily chosen. In practice, identification and validation of the QR model and rotor dynamics is required. The mathematical model requires inclusion of the masses, inertia matrix and lengths of the QR, as well as the drag and thrust constants of the rotors, that are very unlikely to be identical.

As a theoretical extension the influence of model mismatches could be simulated.

Robustness The control in this thesis assumes perfect state feedback. In practice the controller depends on visual feedback or data obtained from an on-board inertial measurement unit. Unlike in simulations, this data will contain noise, uncertainties and possibly drift. Based on a nonlinear geometric approach for a QR without load, [4] includes uncertainties in the translational dynamics and rotational dynamics to prove the robustness against unstructured uncertainties. This work could be extended to a QR-Load system to investigate the effects of non-perfect state feedback.

Due to uncertainties In what way would parameter choice in the controllers affect robustness?
To test the controller for

How to estimate states?

Parameter Estimation can be done by

State Estimation can be done by

Drawback: assumes all states to be known

Model based. What if analytical model is not accurate?

What parameters must be

6-2-2 Minimum Snap Trajectory Generation

The trajectories described in Section 4-2 were arbitrarily generated by hand to test the performance of the controller in different situations. Whenever more complex trajectories are desired, or when an optimal trajectory is required, this approach is no longer efficient and too complex to solve by hand. A recommended extension to this thesis is the automatic generation of a trajectory. This approach is presented by [20] and applied in [7, 21]. A QP problem is solved by minimizing the second derivative of the acceleration (snap), which guarantees a smooth optimal trajectory. The QP allows inclusion of constraints, such as maximum inputs and checkpoints in trajectories, by formulating these as constraints of the QP problem. Furthermore, it is proven that the system is *differential flat*, meaning that all states and inputs

can be expressed in terms of only four states and their derivatives. This property is used to transform the high-dimensional optimization problem into a four-dimensional problem.

6-2-3 Hybrid System

This thesis is only focused on the subsystem where the tension in the cable is non-zero. A possible extension is to apply hybrid control, such that the controller is able to switch between two subsystem models whenever the cable tension switches between zero and non-zero. A trajectory generation method that accounts for the switching dynamics of the hybrid system is presented in [7]. In [15, 7, 21] both subsystems are expressed in the form of one hybrid model.

Appendix A

Appendix

A-1 Derivation of Equations of motion

A-1-1 Load Dynamics

Let x_{CM} denote the position of the center of mass of the combined Quadrotor-Load system, expressed in $\{\mathcal{I}\}$. Which can be found by

$$\begin{aligned} m_Q(x_Q - x_{CM}) + m_L(x_L - x_{CM}) &= 0 \\ (m_Q + m_L)x_{CM} &= m_Q x_Q + m_L x_L \end{aligned} \tag{A-1}$$

Applying Newton's laws of motion to (A-1) and inserting (2-14) gives the

$$\begin{aligned} (m_Q + m_L)\ddot{x}_{CM} &= fRe_3 - (m_Q + m_L)ge_3 \\ (m_Q + m_L)(\ddot{x}_L + ge_3) &= fRe_3 + m_Q L\ddot{q} \end{aligned} \tag{A-2}$$

Here comes the derivation of \ddot{q} , obtained by geometric mechanics.

A-2 LQR controller

A-2-1 Modeling

The linearized model is written into a first order ODE of the form

$$\dot{\mathbf{x}} = A\mathbf{x} + Bu \tag{A-3}$$

$$y = C\mathbf{x} + Du \tag{A-4}$$

with the following state- and input vectors

$$\begin{aligned} \mathbf{x} &= [x \ y \ z \ \phi \ \theta \ \psi \ \phi_L \ \theta_L \ \dot{x} \ \dot{y} \ \dot{z} \ \dot{\phi} \ \dot{\theta} \ \dot{\psi} \ \dot{\phi}_L \ \dot{\theta}_L]^T \\ u &= [f \ M_\phi \ M_\theta \ M_\psi]^T \end{aligned} \tag{A-5}$$

The model is linearized about the hovering flight mode. All translational and rotational velocities are zero during hover. The positional states and the yaw angle do not affect the dynamics, and are set equal to zero. A thrust input $u_1 = g(m_Q + m_L)$ is required to maintain hover, and all other control inputs are set equal to zero. The states and inputs in the equations of motion are substituted by an initial condition and a perturbation

$$\dot{\mathbf{x}} \rightarrow \dot{\mathbf{x}}_0 + \delta\dot{\mathbf{x}}, \quad \mathbf{x} \rightarrow \mathbf{x}_0 + \delta\mathbf{x}, \quad u \rightarrow u_0 + \delta u \quad (\text{A-6})$$

$$\begin{aligned} \mathbf{x}(0) &= \mathbf{0} \\ u(0) &= [g(m_Q + m_L) \quad 0 \quad 0 \quad 0]^T \end{aligned} \quad (\text{A-7})$$

The linearized equations of motion are rearranged into Equation A-8 and substituted in Equation A-3.

$$[\text{content...}] \begin{bmatrix} \delta\ddot{x} \\ \delta\ddot{y} \\ \delta\ddot{z} \\ \delta\ddot{\phi} \\ \delta\ddot{\theta} \\ \delta\ddot{\psi} \\ \delta\ddot{\phi}_L \\ \delta\ddot{\theta}_L \end{bmatrix} + [\text{content...}] \begin{bmatrix} \delta x \\ \delta y \\ \delta z \\ \delta\phi \\ \delta\theta \\ \delta\psi \\ \delta\phi_L \\ \delta\theta_L \end{bmatrix} = [\text{content...}] \begin{bmatrix} \delta u_1 \\ \delta u_2 \\ \delta u_3 \\ \delta u_4 \end{bmatrix} \quad (\text{A-8})$$

$$1 \quad \text{LQRA} =$$

$$\text{LQRB} =$$

The tuning parameters of the LQR controller are chosen as follows

$$\begin{aligned} Q &= \text{diag}(10 \quad 10 \quad 100, \quad 1 \quad 1 \quad 1, \quad 1 \quad 1, \quad 1 \quad 1 \quad 1, \quad 1 \quad 1 \quad 1, \quad 1 \quad 1) \\ R &= \text{diag}(0.044, \quad 1.56, \quad 1.56, \quad 1.56) \end{aligned} \quad (\text{A-9})$$

Matlab command `lqr(LQRA,LQRB,Q,R)` generates the following gain matrix K

$$K =$$

A-3 Classical Modeling

This section describes the derivation of the model by using classical modeling techniques.

When assuming small angle maneuvers, *Euler-angles* can be used to locally parameterize the orientation of the body-fixed reference coordinate frame with respect to the inertial reference coordinate frame. Simple linear controllers are often based on a linearized dynamical model, applying this small angles assumption.

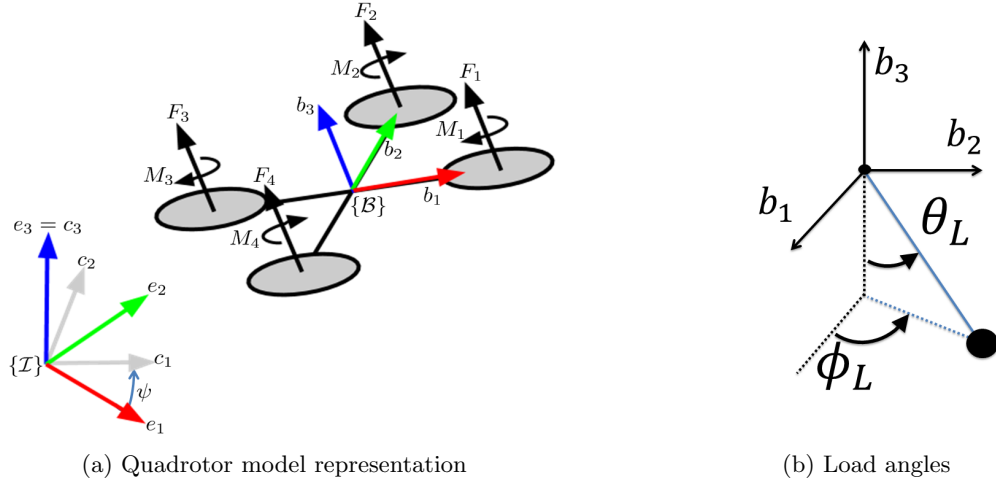


Figure A-1: Model representation

The following equations of motion follow from Newton's law.

$$\begin{aligned}
 \dot{x}_Q &= v_Q \\
 m_Q \dot{v}_Q &= f R e_3 - m_Q g e_3 - T q \\
 \dot{x}_L &= v_L \\
 m_L \dot{v}_L &= -m_L g e_3 + T q
 \end{aligned} \tag{A-10}$$

where $x_Q = x_L - Lq$. T is the cable tension, defined by $T = |f|q$, where $|f| = m_L \dot{v}_L$ is the magnitude of the force.

Because Euler-Angles are used, a function is required that maps a vector of the Z-X-Y Euler angles to its rotation matrix $R \in SO(3)$, which is denoted as [18]

$$R_{ZXY}(\phi, \theta, \psi) = \begin{bmatrix} c_\psi c_\theta - s_\phi s_\psi s_\theta & -c_\phi s_\psi & c_\psi s_\theta + c_\theta s_\phi s_\psi \\ c_\theta s_\psi + c_\psi s_\phi s_\theta & c_\phi c_\psi & s_\psi s_\theta - c_\psi c_\theta s_\phi \\ -c_\phi s_\theta & s_\phi & c_\phi c_\theta \end{bmatrix} \tag{A-11}$$

The Z-X-Y Euler angles rotate $\{\mathcal{B}\}$, as can be seen in Figure A-1a. The first rotation by yaw angle ψ is around the z-axis of $\{\mathcal{I}\}$. Next is the rotation by roll angle ϕ , and the last rotation is by pitch angle θ .

The unit vector q from the QR to the load is represented in $\{\mathcal{B}\}$. Define ϕ_L as the rotation of the load around the z-axis, measured from \vec{b}_1 , and θ_L is the angle between the cable and the z-axis of $\{\mathcal{B}\}$, see Figure A-1b. The Cartesian coordinates can be retrieved through

$$x_L = x_Q + qL \tag{A-12}$$

where

$$q = \begin{bmatrix} s_{\theta_L} c_{\phi_L} \\ s_{\theta_L} s_{\phi_L} \\ -c_{\theta_L} \end{bmatrix} \tag{A-13}$$

Differentiating Equation A-12 and A-13 gives

$$\ddot{x}_L = \ddot{x}_Q + \ddot{q}L$$

$$\ddot{q} = \begin{bmatrix} \ddot{\theta}_L c_{\theta_L} c_{\phi_L} - \ddot{\phi}_L s_{\theta_L} s_{\phi_L} - \dot{\phi}_L^2 s_{\theta_L} c_{\phi_L} - \dot{\theta}_L^2 s_{\theta_L} c_{\phi_L} - 2\dot{\theta}_L \dot{\phi}_L c_{\theta_L} s_{\phi_L} \\ \ddot{\theta}_L c_{\theta_L} s_{\phi_L} + \ddot{\phi}_L s_{\theta_L} c_{\phi_L} - \dot{\phi}_L^2 s_{\theta_L} s_{\phi_L} - \dot{\theta}_L^2 s_{\theta_L} s_{\phi_L} + 2\dot{\theta}_L \dot{\phi}_L c_{\theta_L} c_{\phi_L} \\ \ddot{\theta}_L s_{\theta_L} + \dot{\theta}_L^2 c_{\theta_L} \end{bmatrix} \quad (\text{A-14})$$

$$\ddot{x}_Q = \frac{1}{m_Q} (f(c_\psi s_\theta + c_\theta s_\phi s_\psi) - T s_{\theta_L} c_{\psi_L})$$

$$\ddot{y}_Q = \frac{1}{m_Q} (f(s_\psi s_\theta - c_\psi c_\theta s_\phi) - T s_{\theta_L} s_{\psi_L})$$

$$\ddot{z}_Q = \frac{1}{m_Q} (f(c_\phi c_\theta) - T c_{\theta_L}) - g \quad (\text{A-15})$$

A-4 Derivation Error dynamics

Recall the angular velocity tracking error e_Ω , from this follows

$$e_\Omega = \Omega - R^T R_d \Omega_d,$$

$$\hat{e}_\Omega = \hat{\Omega} - R^T R_d \hat{\Omega}_d R_d^T R \quad (\text{A-16})$$

Equation A-16 is used to derive the attitude velocity error \dot{e}_R as follows

$$e_R = \frac{1}{2} (R_d^T R - R^T R_d)^\vee,$$

$$\dot{e}_R = \frac{1}{2} (\dot{R}_d^T R + R_d^T \dot{R} - \dot{R}^T R_d - R^T \dot{R}_d)^\vee$$

$$= \frac{1}{2} ((R_d \hat{\Omega}_d)^T R + R_d^T (R \hat{\Omega}) - (R \hat{\Omega})^T R_d - R^T (R_d \hat{\Omega}_d))^\vee$$

$$= \frac{1}{2} (-\hat{\Omega}_d R_d^T R + R_d^T R \hat{\Omega} + \hat{\Omega} R^T R_d - R^T R_d \hat{\Omega}_d)^\vee \quad (\text{A-17})$$

$$= \frac{1}{2} (R_d^T R (\hat{\Omega} - R^T R_d \hat{\Omega}_d R_d^T R) + (\hat{\Omega} - R^T R_d \hat{\Omega}_d R_d^T R) R^T R_d)^\vee$$

$$= \frac{1}{2} (R_d^T R \hat{e}_\Omega + \hat{e}_\Omega R^T R_d)^\vee$$

$$= \frac{1}{2} (tr[R^T R_d] I - R^T R_d) e_\Omega \equiv C(R_d^T R) e_\Omega$$

It can be shown that $\|C(R_d^T R)\|_2 \leq 1$ for any $R_d^T R \in SO(3)$.

From that follows $\|\dot{e}_R\| \leq \|e_\Omega\|$.

$$\dot{e}_\Omega = \dot{\Omega} - \dot{R}^T R_d \Omega_d - R^T \dot{R}_d \Omega_d - R^T R_d \dot{\Omega}_d$$

$$= \dot{\Omega} - (R \hat{\Omega})^T R_d \Omega_d - R^T (R_d \hat{\Omega}_d) \Omega_d - R^T R_d \dot{\Omega}_d$$

$$= \dot{\Omega} + \hat{\Omega} R^T R_d \Omega_d - R^T (R_d \hat{\Omega}_d) \Omega_d - R^T R_d \dot{\Omega}_d$$

$$= J^{-1}(-\Omega \times J\Omega + M) + \hat{\Omega} R^T R_d \Omega_d - R^T R_d \dot{\Omega}_d \quad (\text{A-18})$$

where $\hat{\Omega}_d \Omega_d = \Omega_d \times \Omega_d = 0$.

A-5 Figures



Figure A-2: Simulink Command Filter

Bibliography

- [1] R. P. K. Jain and T. Keviczky, “MSc Thesis: Transportation of Cable Suspended Load using Unmanned Aerial Vehicles: A Real-time Model Predictive Control approach,” 2015.
- [2] S. Sadr, S. A. A. Moosavian, and P. Zarafshan, “Dynamics Modeling and Control of a Quad-rotor Helicopter,” *Journal of Robotics, Hindawi Publishing Corporation*, vol. 2014, no. August 2016, 2014.
- [3] T. Lee, M. Leok, and N. H. Mcclamroch, “Geometric Tracking Control of a Quadrotor UAV on $SE(3)$,” *49th IEEE Conference on Decision and Control*, no. 3, pp. 5420–5425, 2010.
- [4] F. Goodarzi, D. Lee, and T. Lee, “Geometric nonlinear PID control of a quadrotor UAV on $SE(3)$,” *Control Conference (ECC), 2013 European*, pp. 3845–3850, 2013.
- [5] K. Sreenath, N. Michael, and V. Kumar, “Trajectory generation and control of a quadrotor with a cable-suspended load - A differentially-flat hybrid system,” in *Proceedings - IEEE International Conference on Robotics and Automation*, pp. 4888–4895, 2013.
- [6] K. Sreenath, T. Lee, and V. Kumar, “Geometric control and differential flatness of a quadrotor UAV with a cable-suspended load,” in *Proceedings of the IEEE Conference on Decision and Control*, pp. 2269–2274, 2013.
- [7] S. Tang, “Aggressive Maneuvering of a Quadrotor with a Cable-Suspended Payload,” tech. rep., University of Pennsylvania Philadelphia, Pennsylvania, 2014.
- [8] N. Chaturvedi, “Rigid-Body Attitude Control,” *IEEE Control Systems*, vol. 31, no. 3, pp. 30–51, 2011.
- [9] R. M. Murray, Z. Li, and S. S. Sastry, *A Mathematical Introduction to Robotic Manipulation*, vol. 29. 1994.
- [10] T. Lee, *Computational Geometric Mechanics and Control of Rigid Bodies*. PhD thesis, The University of Michigan, 2008.

- [11] T. L. T. Lee, N. McClamroch, and M. Leok, "A lie group variational integrator for the attitude dynamics of a rigid body with applications to the 3D pendulum," *Proceedings of 2005 IEEE Conference on Control Applications, 2005. CCA 2005.*, pp. 962–967, 2005.
- [12] T. Lee, M. Leok, and N. H. McClamroch, "Lagrangian mechanics and variational integrators on two-spheres," *International Journal for Numerical Methods in Engineering*, vol. 79, no. 9, pp. 1147–1174, 2009.
- [13] T. Lee, M. Leok, and N. H. McClamroch, "Stable Manifolds of Saddle Points for Pendulum Dynamics on S^2 and $SO(3)$," p. 9, 2011.
- [14] F. Bullo and A. D. Lewis, *Geometric control of mechanical systems: modeling, analysis, and design for simple mechanical control systems*. Springer, 2005.
- [15] K. Sreenath, Taeyoung Lee, and V. Kumar, "Geometric control and differential flatness of a quadrotor UAV with a cable-suspended load," in *52nd IEEE Conference on Decision and Control*, pp. 2269–2274, IEEE, dec 2013.
- [16] N. A. Chaturvedi, T. Lee, M. Leok, and N. H. McClamroch, "Nonlinear dynamics of the 3D pendulum," *Journal of Nonlinear Science*, vol. 21, no. 1, pp. 3–32, 2011.
- [17] J. H. Gillula, H. Huang, M. P. Vitus, and C. J. Tomlin, "Design of guaranteed safe maneuvers using reachable sets: Autonomous quadrotor aerobatics in theory and practice," in *Proceedings - IEEE International Conference on Robotics and Automation*, pp. 1649–1654, 2010.
- [18] R. Mahony, V. Kumar, and P. Corke, "Multirotor Aerial Vehicles: Modeling, Estimation, and Control of Quadrotor," *IEEE Robotics & Automation Magazine*, vol. 19, no. 3, pp. 20–32, 2012.
- [19] J. A. Farrell, M. Polycarpou, M. Sharma, and W. Dong, "Command Filtered Backstepping," pp. 1923–1928, 2008.
- [20] D. Mellinger and V. Kumar, "Minimum snap trajectory generation and control for quadrotors," in *Proceedings - IEEE International Conference on Robotics and Automation*, pp. 2520–2525, 2011.
- [21] S. Tang and V. Kumar, "Mixed Integer Quadratic Program Trajectory Generation for a Quadrotor with a Cable-Suspended Payload," *IEEE International Conference on Robotics and Automation (ICRA)*, pp. 2216–2222, 2015.

Nomenclature

ϵ	Tuning parameter to enable rapid exponential convergence of e_R, e_Ω
$\lambda_M(\cdot)$	Maximum eigenvalue
ω_i	Angular speed of rotor i
$\{\mathbf{b}_1, \mathbf{b}_2, \mathbf{b}_3\}$	Unit vectors along the axes of $\{\mathcal{B}\}$
$\{\mathbf{c}_1, \mathbf{c}_2, \mathbf{c}_3\}$	Unit vectors along the axes of $\{\mathcal{C}\}$
$\{\mathbf{e}_1, \mathbf{e}_2, \mathbf{e}_3\}$	Unit vectors along the axes of $\{\mathcal{I}\}$
$\{\mathcal{B}\}$	Body Frame
$\{\mathcal{C}\}$	Intermediary Frame
$\{\mathcal{I}\}$	Inertial World Frame
b	Thrust factor
d	Drag factor
f	Total thrust. $f = \sum_{i=1}^4 F_i$
F_i	Force generated by rotor i
g	Gravitation constant
$J \in \mathbb{R}^3$	Inertia tensor of QR
L	Length of the cable
l	Distance from the rotor to the QR CM
M	Total moment in $\{\mathcal{B}\}$. $M = [M_\phi \quad M_\theta \quad M_\psi]^T$
M_i	Drag moment generated by each propellor

q	Unit vector from QR to Load
x_L	Position of the load
x_Q	Position of the of the QR CM
x_{CM}	Position CM of QR-Load system

Acronyms

QR	Quadrotor
UAV	Unmanned Aerial Vehicle
CM	Center of Mass
DOF	Degree of Freedom
PID	Proportional-Integral-Derivative (Controller)
MPC	Model Predictive Control
LQR	Linear Quadratic Regulator
QP	Quadratic Programming